JOURNAL OF GEOPHYSICAL RESEARCH: PLANETS, VOL. 118, 1–20, doi:10.1002/jgre.20052, 2013

An assemblage of lava flow features on Mercury

Paul K. Byrne,[1] Christian Klimczak,[1] David A. Williams,[2] Debra M. Hurwitz,[3,6] Sean C. Solomon,[1,4] James W. Head,[3] Frank Preusker,[5] and Jürgen Oberst[5]

Received 11 July 2012; revised 26 November 2012; accepted 15 January 2013.

[1] In contrast to other terrestrial planets, Mercury does not possess a great variety of volcanic features, its history of volcanism instead largely manifest by expansive smooth plains. However, a set of landforms at high northern latitudes on Mercury resembles surface flow features documented on Earth, the Moon, Mars, and Venus. The most striking of such landforms are broad channels that host streamlined islands and that cut through the surrounding intercrater plains. Together with narrower, more sinuous channels, coalesced depressions, evidence for local flooding of intercrater plains by lavas, and a first-order analysis of lava flow rates, the broad channels define an assemblage of flow features formed by the overland flow of, and erosion by, voluminous, high-temperature, low-viscosity lavas. This interpretation is consistent with compositional data suggesting that substantial portions of Mercury's crust are composed of magnesian, iron-poor lithologies. Moreover, the proximity of this partially flooded assemblage to extensive volcanic plains raises the possibility that the formation of these flow features may preface total inundation of an area by lavas emplaced in a flood mode and that they escaped complete burial only due to a waning magmatic supply. Finally, that these broad channels on Mercury are volcanic in nature yet resemble outflow channels on Mars, which are commonly attributed to catastrophic water floods, implies that aqueous activity is not a prerequisite for the formation of such distinctive landforms on any planetary body.

Citation: Byrne, P. K., C. Klimczak, D. A. Williams, D. M. Hurwitz, S. C. Solomon, J. W. Head, F. Preusker, and J. Oberst (2013), An assemblage of lava flow features on Mercury, *J. Geophys. Res. Planets*, *118*, doi:10.1002/jgre.20052.

1. Introduction

[2] By returning images of extensive smooth plains deposits within and surrounding the Caloris basin and other large impact basins on Mercury, the Mariner 10 flybys raised the prospect that extensive surface volcanism had occurred on the innermost planet. Some workers considered these deposits to be of impact origin, regarding them as morphologically similar to lunar highland plains known to have been emplaced as fluidized impact ejecta deposits [*Wilhelms*, 1976; *Oberbeck et al*., 1977]. Others viewed embayment relations between Mercury's smooth plains and surrounding terrain, together with estimates of plains volumes far in excess of those expected from impact processes alone, as strong evidence for an origin by volcanism [*Murray et al*., 1975; *Strom et al*., 1975; *Dzurisin*, 1978; *Kiefer and Murray*, 1987; *Robinson and Lucey*, 1997].

[3] Strong support for widespread surface volcanism on Mercury was provided by the MErcury Surface, Space ENvironment, GEochemistry, and Ranging (MESSENGER) spacecraft from observations made during its three Mercury flybys [*Solomon et al*., 2011]. Near-global imaging of the planet revealed extensive smooth plains deposits that showed evidence for sequential embayment of impact basins and ejecta and that were spectrally homogenous but differed in color from surrounding terrain, featured lobate margins morphologically similar to lava flow fronts, partially buried numerous impact craters, and ranged in thicknesses from hundreds of meters to several kilometers [*Head et al*., 2008, 2009a; *Denevi et al*., 2009; *Prockter et al*., 2010]. From flyby data, an especially large region of smooth plains was identified at high northern latitudes [*Denevi et al*., 2009; *Fassett et al*., 2011] (Figure 1, label 1); early results from orbit indicated that, although not obviously related to one or more large impact basins, these plains cover some 6% of Mercury's surface and appear to have been emplaced by low-viscosity, high-effusion lavas in a flood-mode style similar to large basaltic igneous provinces on Earth [*Head et al*., 2011].

[1]Department of Terrestrial Magnetism, Carnegie Institution of Washington, Washington, D.C., USA.
[2]School of Earth and Space Exploration, Arizona State University, Tempe, Arizona, USA.
[3]Department of Geological Sciences, Brown University, Providence, Rhode Island, USA.
[4]Lamont-Doherty Earth Observatory, Columbia University, Palisades, New York, USA.
[5]Institute of Planetary Research, German Aerospace Center, Berlin, Germany.
[6]Lunar and Planetary Institute, Houston, Texas, USA.

Corresponding author: P. K. Byrne, Department of Terrestrial Magnetism, Carnegie Institution of Washington, 5241 Broad Branch Road N.W., Washington, DC 20015–1305, USA. (pbyrne@dtm.ciw.edu)

©2013. American Geophysical Union. All Rights Reserved.
2169-9097/13/10.1002/jgre.20052

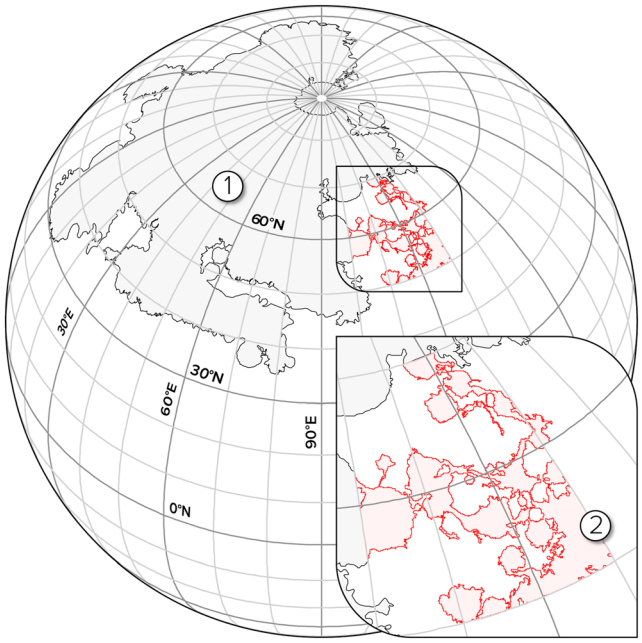

Figure 1. An orthographic sketch centered at 45°N, 90°E, showing the locations and spatial extent of (label 1) the northern smooth plains [*Head et al*., 2011], outlined in black, and (label 2) the contiguous smooth plains deposits described in this study, outlined in red.

[4] A major challenge associated with understanding the development of large volcanic provinces, such as Mercury's northern smooth plains, is the burial of source vents and flow-related features by successive lavas, rendering the determination of flow directions, unit thicknesses, and detailed emplacement histories difficult. Such burial adds to the paucity of primary volcanic landforms on Mercury [*Strom et al*., 1975]. Although smooth plains are abundant, the surface of the innermost planet lacks the large shield constructs and abundant erosional rilles commonly observed on other volcanic worlds [e.g. *Hulme*, 1973; *Whitford-Stark and Head*, 1977; *Greeley and Spudis*, 1981; *Head et al*., 1992; *Schenk et al*., 2004], and evidence for intrusive activity is also scarce [*Head et al*., 2009b; *Klimczak et al*., 2010].

[5] Mercury is not entirely without volcanic flow features, however, as evinced by the recent discovery of an assemblage of channels, coalesced depressions, and related landforms that escaped burial and are proximal to the southeastern margin of the northern smooth plains deposits [*Byrne et al*., 2011; *Head et al*., 2011] (Figure 1, label 2). Together with other candidate lava flow features elsewhere on Mercury [*Hurwitz et al*., 2013], these landforms can provide important information about the behavior, duration, and volume of surface volcanism on Mercury that, in turn, serves as a basis for understanding the development of smooth plains deposits across the planet.

[6] In this paper, we document in detail this northern flow-feature assemblage, which we define as a network of interconnected smooth plains, and we characterize the broad and narrow channels that feature streamlined islands, as well as flooded impact basins and craters, candidate calderas, and evidence of partial resurfacing of adjacent intercrater plains terrain. Taking key morphological measurements for a single broad-channel–flooded-basin pair, we follow the approach of *Williams et al*. [2001a] to calculate a range of lava flow rates through the channel and thus fill times for the downstream flooded basin, providing first-order quantitative data for lava flows on Mercury. We also review an apparent topographic anomaly within two broad channels that suggests that long-wavelength modification of the regional topography has occurred since channel formation. Finally, we synthesize our observations and relate the development of the flow feature assemblage to the volcanic history of Mercury in general.

2. Methods

[7] The basis for our photogeological mapping was a Mercury Dual Imaging System (MDIS) [*Hawkins et al*., 2007] wide-angle camera (WAC) global image mosaic [cf. *Becker et al*., 2012], with a mean resolution of 250 m/px. This base map was supplemented by MDIS narrow-angle camera (NAC) high-resolution targeted images (at ~25 m/px resolution) for areas of specific interest. All data were projected and analyzed within an ESRI® ArcMap™ 10.0 geographical information system (GIS) (Figure 2).

[8] Our mapping approach involved delineating the margins of landforms we attributed to lava flow and yielded an interconnected network of outlines that encloses the smooth plains deposits within the northern assemblage (Figure 3). These outlines served as the basis for such morphometric determinations as channel length, flooded basin diameter, and coalesced depression diameter. A gridded digital terrain model (DTM), derived from Mercury Laser Altimeter (MLA) topographic profiles [*Zuber et al*., 2012], provided elevation data where coverage permitted and from which we identified regional topographic trends and downslope directions.

[9] To calculate lava flow rates through a single broad channel, Angkor Vallis, we employed a set of equations for confined (channel- or tube-fed) flows, taken from *Williams et al*. [2001a], to calculate iteratively the Reynolds number (*Re*), friction coefficient (λ), and flow velocity (*u*) for two candidate lava viscosities. By then taking an estimate for the volume of volcanic fill within a basin at the assumed downstream end of Angkor Vallis, we determined corresponding basin fill times (see section 3.2).

3. Results

3.1. Photogeological Mapping

[10] Our study area encompassed the northern flow feature assemblage, which lies almost entirely between the 50°N and 70°N parallels and the 90°E and 120°E meridians (Figure 2). The flow features themselves are situated within a region of rough, intercrater plains [e.g., *Trask and Guest*, 1975; *Denevi et al*., 2009]. The northern plains documented by *Head et al*. [2011] lie to the northwest, and the Caloris exterior plains [e.g., *Murchie et al*., 2008] are to the southeast.

[11] The boundary between intercrater plains terrain and topographically lower, contiguous smooth plains material is shown in the physiographic map in Figure 3. This boundary also outlines kipukas (sections of high-standing, older terrain that have been completely surrounded by younger lavas and so form islands within channels and flooded basins in the area). Several coalesced depressions are also shown on the

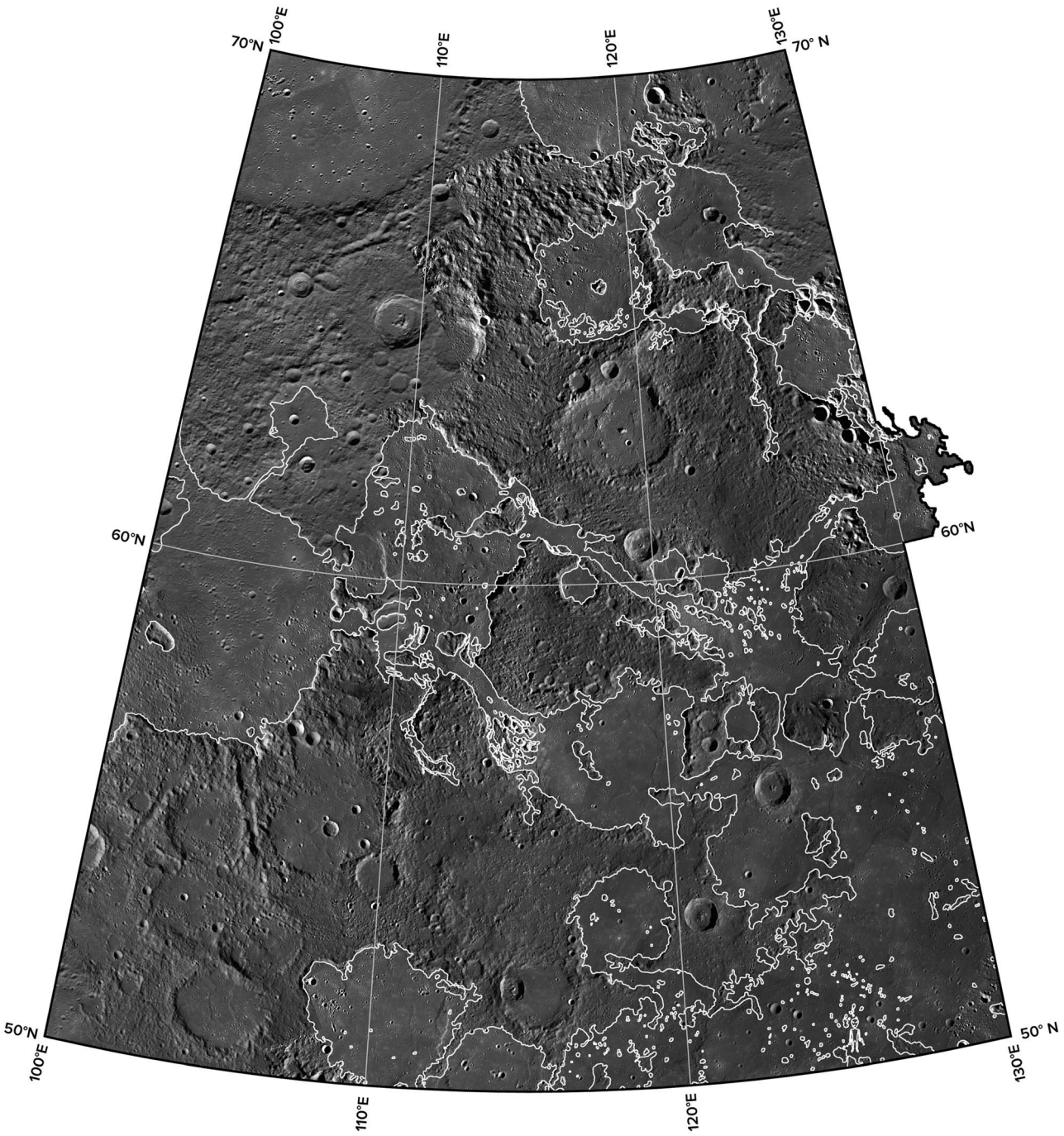

Figure 2. An MDIS WAC and NAC photomosaic of our study area, which is bounded by the 50°N and 70°N parallels and the 90°E and 120°E meridians. The area of contiguous smooth plains in this area is outlined in white. The image is an orthographic projection centered at 60°N, 115°E. The WAC portions of this mosaic are extracts of the global monochrome base map [cf. *Becker et al*., 2012].

map. The area of contiguous smooth plains encompassed by this boundary is approximately 192,000 km^2. We show the locations of Figures 5–10 in Figure 4.

3.1.1. Broad Channels

[12] Perhaps the most striking surface-flow landforms in this region are five broad, linear channels that interconnect a number of flooded impact basins and craters (Figures 5a–5e). Named Angkor, Cahokia, Caral, Paestum, and Timgad Valles, and with a combined area of 7735 km^2, these channels constitute an area equal to some 4% of the contiguous smooth plains. The channels are characterized by generally smooth floors at the resolution of the WAC base map (Figures 5a–5e, label 1), but NAC images show these floors to be populated with hundreds of small primary and secondary impact craters, substantial widths relative to lengths, and steep sides. No stratigraphic layering, lineations, or similar structural detail is visible along the channel walls in high-resolution images, but at least one channel features terraces along its

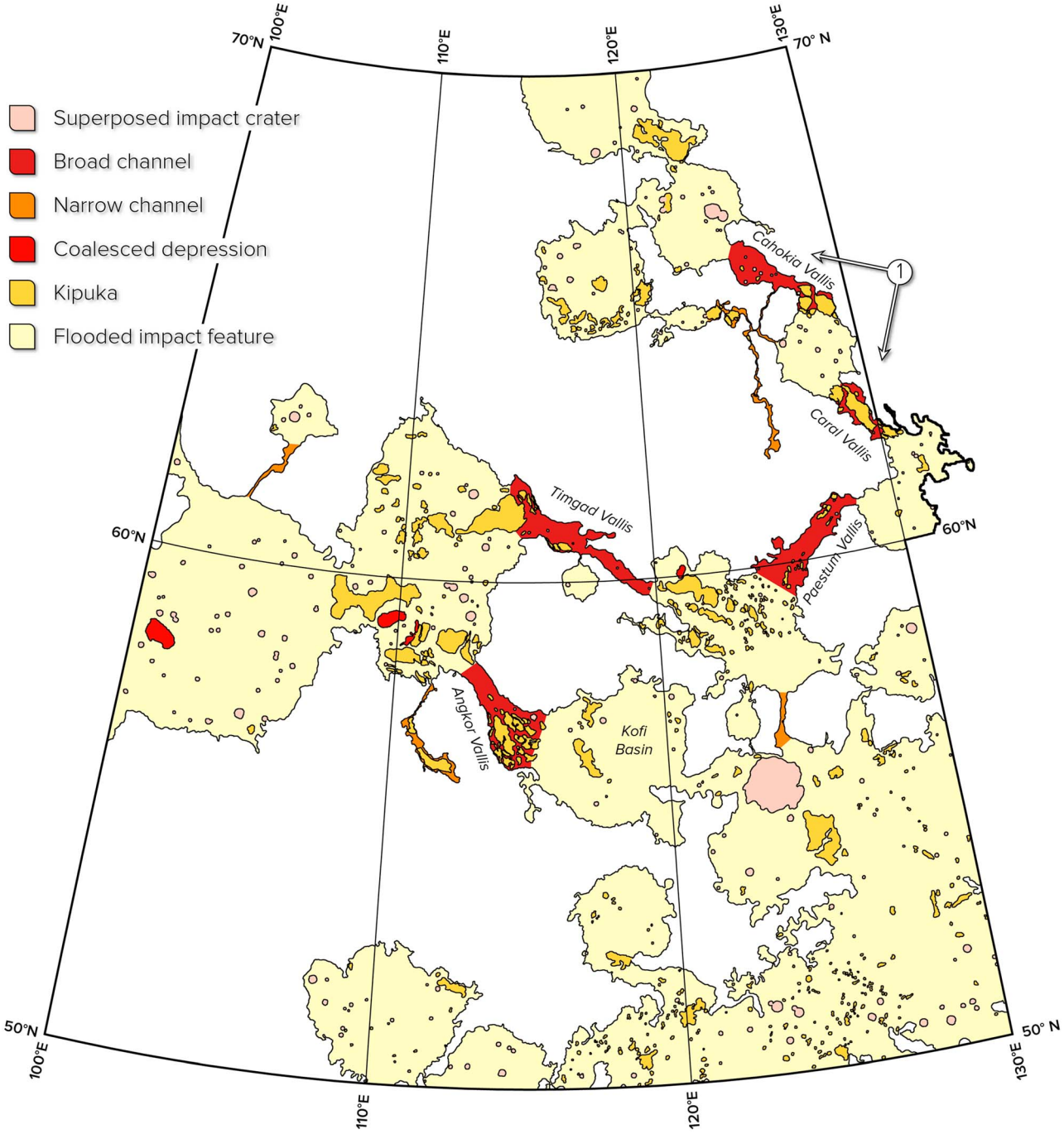

Figure 3. A physiographic map of the study area, color-coded according to feature. The smooth plains are shown in pale yellow and are outlined in black. The most prominent flow-related features in the area are five broad channels (Angkor, Cahokia, Caral, Paestum, and Timgad Valles, shown in dark red), which are accompanied by narrow channels (orange), kipukas (dark yellow), and coalesced depressions (red). Two of the broad channels (indicated by label 1) may originally have been a single channel. Impact craters superposed upon the smooth plains units are shown in pink. The map projection is the same as for Figure 2.

margins (Angkor Vallis: Figure 5a, label 2), and several display a furrowed or ridged texture along their floor (Figures 5a–5c, label 3). Two channels in the eastern portion of the region (Cahokia and Caral Valles: Figures 5b and 5c) intersect a crater ~65 km in diameter and may originally have been a single, contiguous feature (Figure 3, label 1). Key morphometric data for these channels are given in Table 1.

[13] Although the region as a whole is replete with kipukas, of particular interest are those located within the valles, shown in Figure 6. Many of these channel-hosted kipukas are elongate and aligned approximately parallel to the host channel's long axis, whereas some have a lenticular planform. As with the channel walls, NAC images do not reveal any stratigraphic or linear details along the sides of

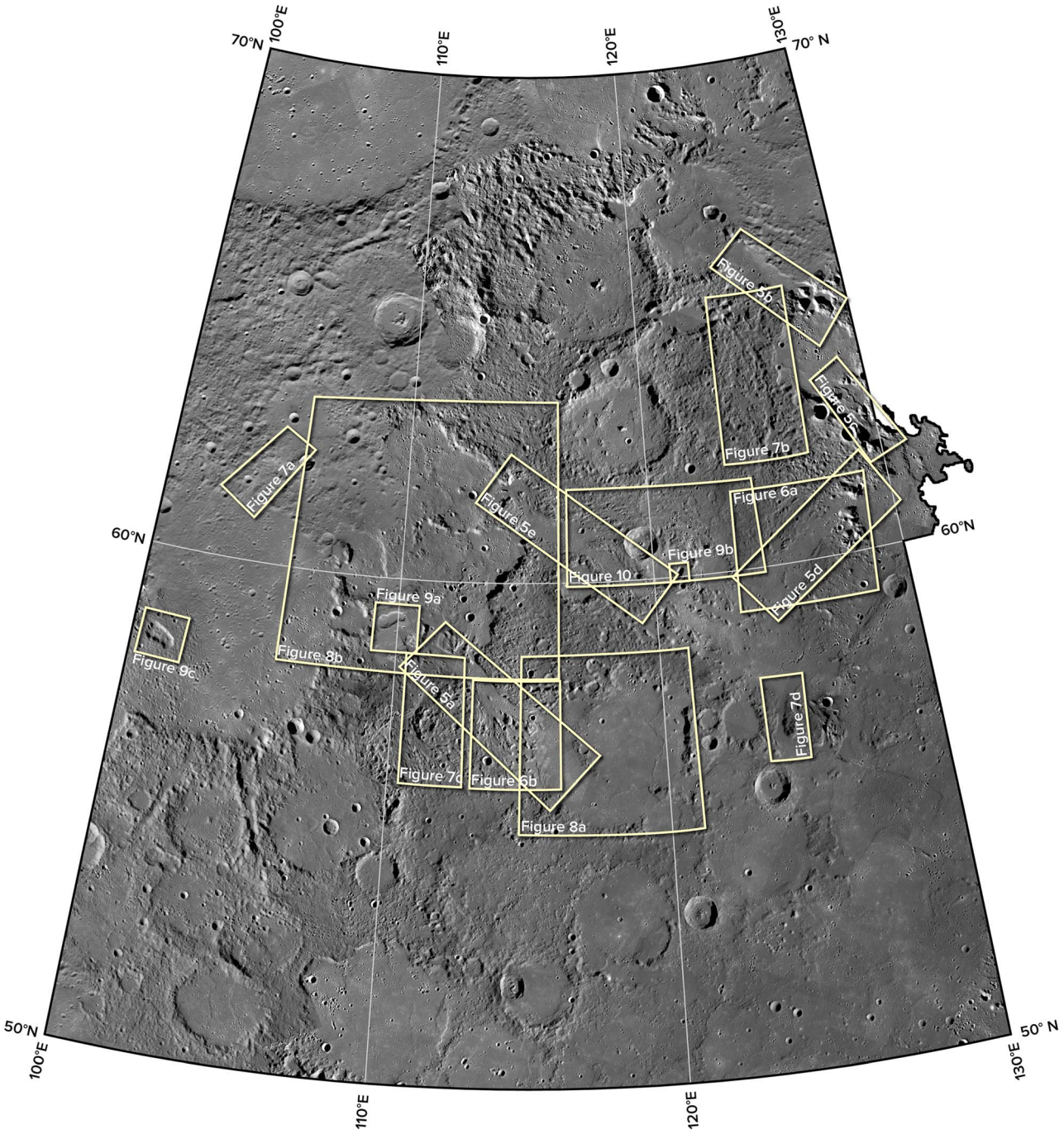

Figure 4. The locations of Figures 5–10 are shown on the MDIS WAC and NAC photomosaic illustrated in Figure 3.

channel-hosted islands. We note, however, that the forms of these islands often appear softened, and there is no pronounced change in slope where they meet the channel floors. In at least one location, where Angkor Vallis joins a flooded basin, the kipukas within that channel are arrayed in a splay-like pattern that opens out into the basin (Figure 6b). MLA topographic data indicate that the heights of channel-hosted islands broadly correspond to the elevation of the surrounding intercrater plains; their plan-view widths and lengths vary but are typically on the order of several kilometers.

3.1.2. Narrow Channels

[14] The area hosts five additional channel-like landforms (Figures 7a–7d), but these features are more sinuous and more narrow (with respect to their length) than their broader counterparts. In many places, the margins of these narrow channels are indistinct, and with one exception the narrow channels do not contain streamlined islands of earlier, intercrater plains material within their extents. Three of the narrow channels link flooded impact craters and are fully integrated into the flow assemblage, whereas the remaining two narrow channels join the assemblage at one end only

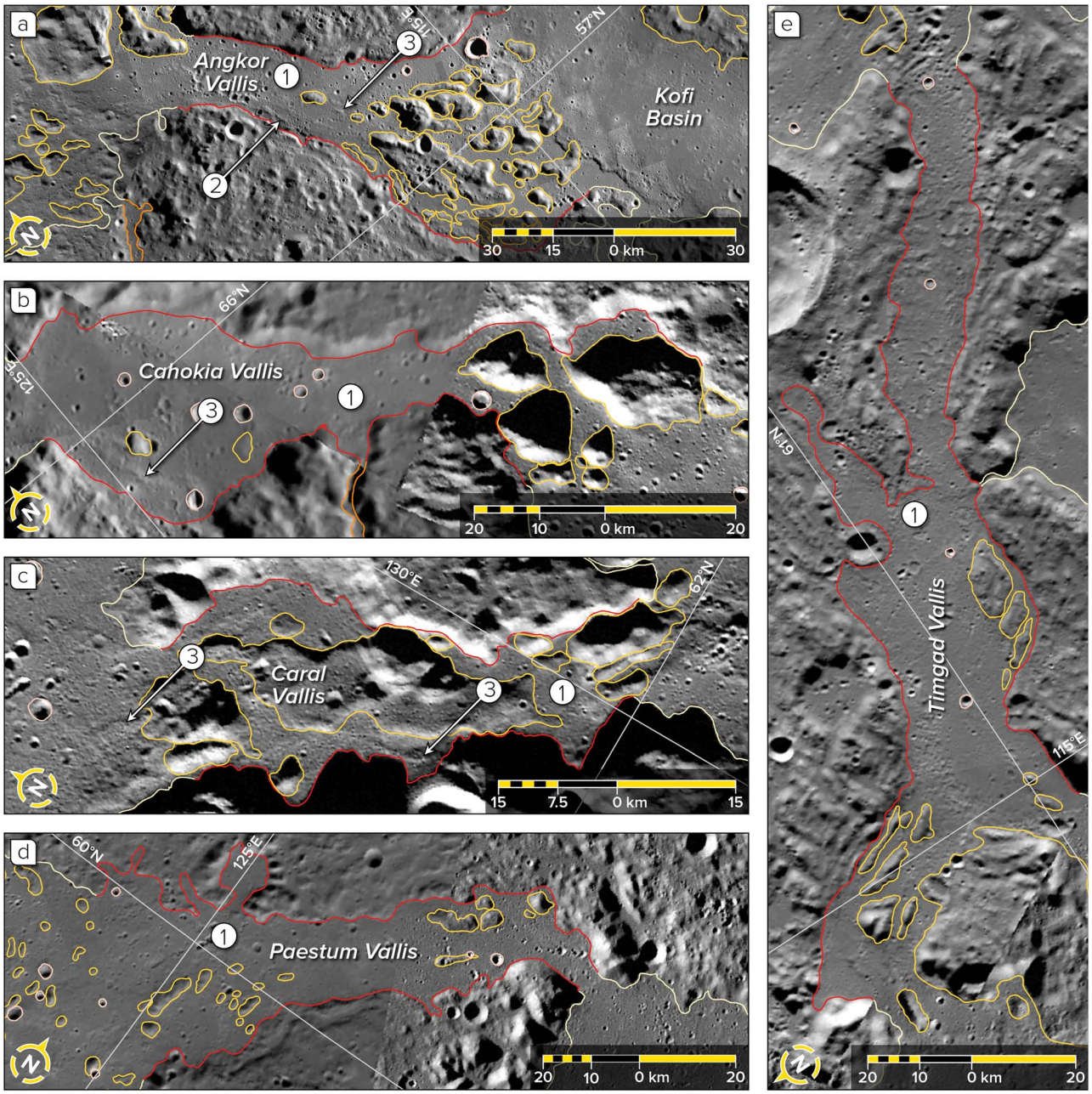

Figure 5. The five broad channels—Angkor, Cahokia, Caral, Paestum, and Timgad Valles—in our study area. Each flow-related feature outline in Figures 5–10 is color-coded according to the key in Figure 3. Broad channels have characteristically smooth floors (label 1), with one displaying terraced margins (label 2), and several showing furrowed floors (label 3). Azimuthal equidistant projections, centered as follows: (a) 57.4°N, 114.1°E; (b) 65.5°N, 127.4°E; (c) 62.6°N, 129.5°E; (d) 60.4°N, 126.4°E; and (e) 60.8°N, 117.2°E.

(their opposite ends are not well defined, instead appearing to merge with the surrounding terrain). Two of the channels intersect one another (Figure 7b, labels 1 and 2). The narrow channels have a combined area of 1525 km^2 (0.8% of the area of contiguous smooth plains). Key morphometric values for narrow channels are given in Table 1.

3.1.3. Flooded Impact Features

[15] Coalesced and channel-linked impact features define the bulk (approximately 95%) of the locations of contiguous smooth plains in which the northern flow assemblage lies (Figure 8). Some impact features retain a near-circular outline (Figure 8a), whereas the perimeters of others have been breached and heavily modified or even obliterated through subsequent impacts and now coalesce with neighboring features (Figure 8b). Although the total is difficult to determine unequivocally, at least 20 interconnected impact basins and craters greater than 50 km in diameter are encompassed in this study region. (We adopt the measurements and nomenclature of *Pike* [1988], updated by *Baker et al.* [2011] with MESSENGER data, and although there is a range of diameters over which multiple crater forms can be seen, for simplicity here we designate impact structure less than ~100 km in diameter as craters, and

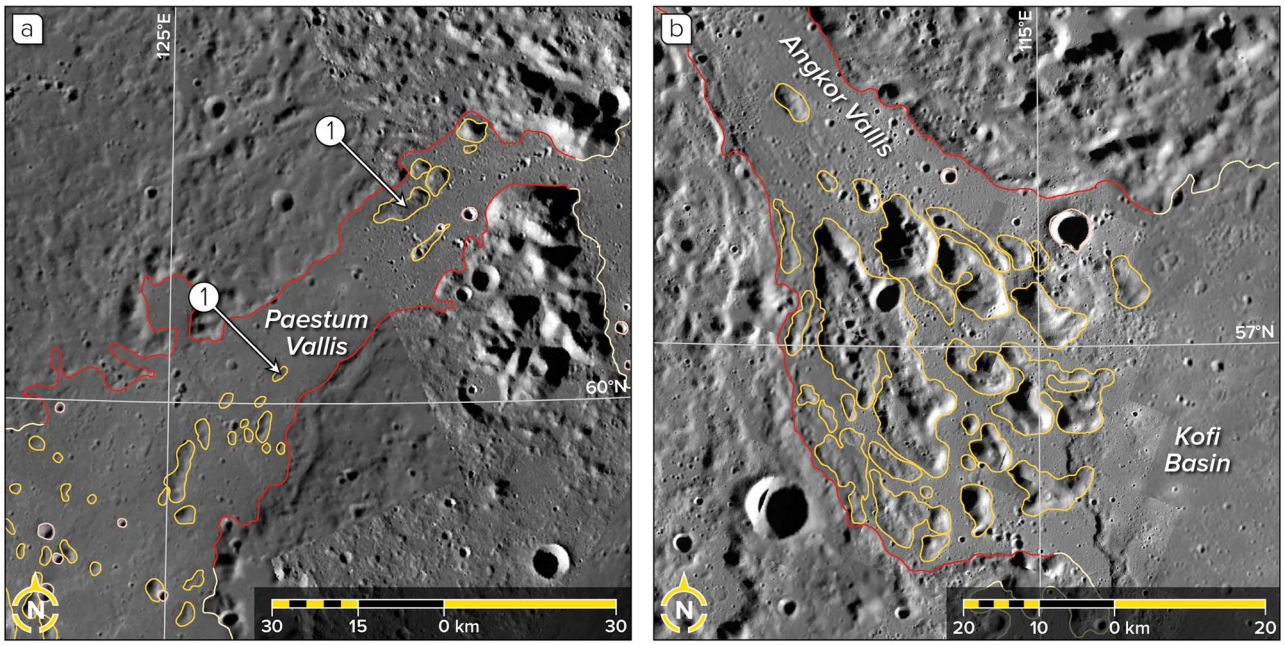

Figure 6. Two examples of kipukas in this area. (a) A large number of kipukas in Paestum Vallis are streamlined in a direction parallel to the channel's long axis (label 1). Azimuthal equidistant projection, centered at 60.3°N, 126.2°E. (b) The kipukas at the southern end of Angkor Vallis have a range of azimuths and form a splay-like pattern at the channel's entrance. Azimuthal equidistant projection, centered at 57°N, 114.6°E.

those greater than that diameter as basins.) Where central peaks, peak rings, or impact rims are evident, such features are almost always partially buried (e.g., Figures 8a and 8b, label 1); in some places, they are entirely absent. Linear, positive-relief landforms that bear a strong resemblance to contractional tectonic landforms (wrinkle ridges and lobate scarps) are widespread in flooded basins (Figures 8a and 8b, label 2). Though superficially resembling lava flow fronts, these structures have differences in elevation of 400–600 m across their leading edges, values consistent with those of ridges and scarps elsewhere on Mercury. In general, these features show no preferred orientations, vergences, or distributions, nor are they aligned with tectonic features outside the flow assemblage. In places, however, we note arcuate ridges and scarps that appear concentric to the basin in which they occur (Figure 8a, label 3).

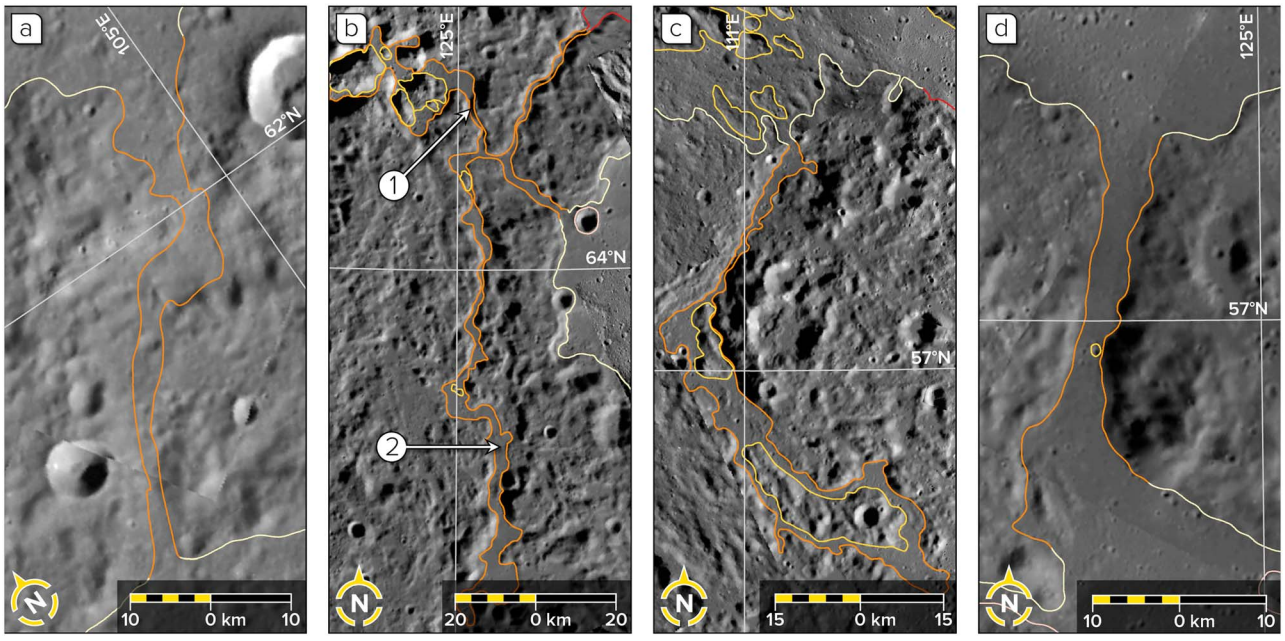

Figure 7. The five narrow channels described in this study. Azimuthal equidistant projections, centered as follows: (a) 61.9°N, 104.3°E; (b) 63.8°N, 125.3°E; (c) 56.9°N, 111°E; and (d) 57°N, 124.2°E.

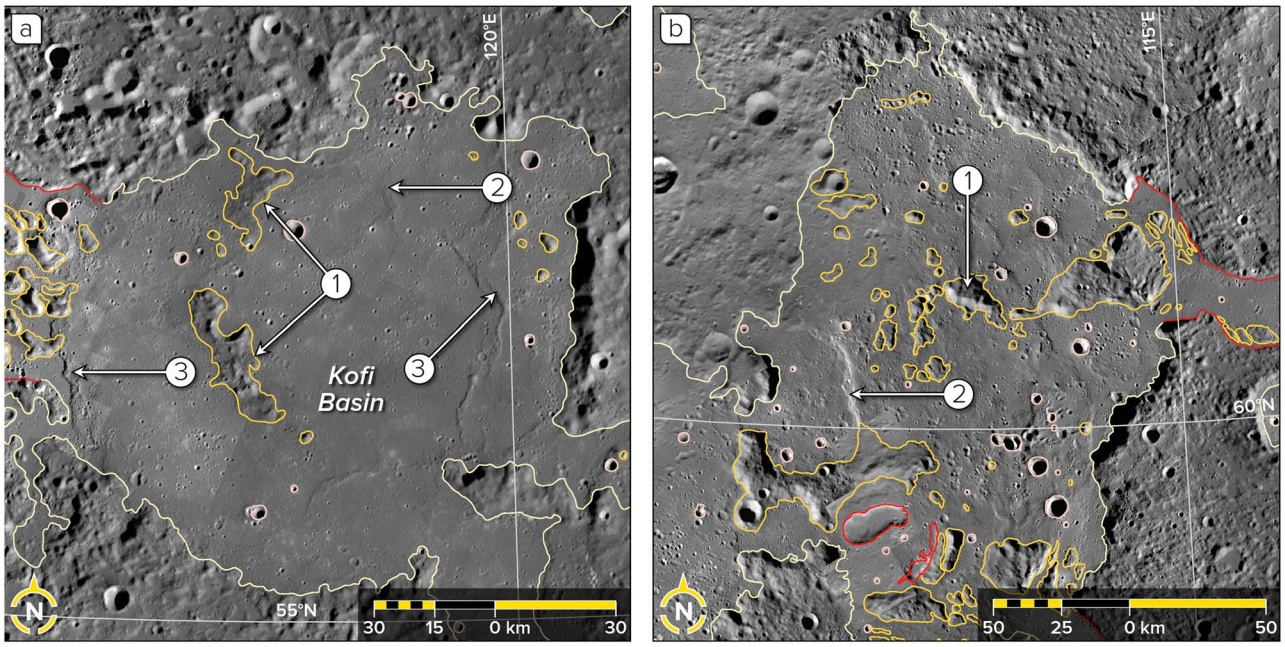

Figure 8. Two examples of coalesced and flooded impact features. (a) Kofi basin, 136 km in diameter, has a near-circular outline, remnants of which may be its peak ring or the rim of a smaller, superposed basin (label 1), and probable contractional tectonic structures (label 2) that in part follow the basin's perimeter (label 3). Azimuthal equidistant projection, centered at 56.5°N, 118°E. (b) A number of coalesced impact features with an isolated remnant of a central peak, peak ring, or rim material (label 1), along with contractional tectonic features (label 2). Azimuthal equidistant projection, centered at 61°N, 111°E.

3.1.4. Coalesced Depressions

[16] At three sites within the contiguous smooth plains lie four flat-floored, elongate depressions (Figures 9a–9c; see also Figures 2 and 3 in a companion paper by *Hurwitz et al.* [2013]). These features have scalloped, irregular outlines (Figures 9a–9c, label 1), and one kidney-shaped depression appears to have a smaller, circular pit nested within it (Figure 9a, label 2). Other than the northwest depression in Figure 8a, which features a narrow, low-relief rim about its perimeter, these landforms show no evidence of raised rims. High-resolution images show a faint stratigraphic layering along the northern wall of this depression (Figure 9a, inset), but no such layering is apparent within the other pits. NAC data do, however, indicate that the edges of each depression are rounded and smooth. Although these pit structures are superposed upon the surrounding smooth plains units, in no cases do resolvable lava flows issue from the pits themselves. Morphological data for these depressions are given in Table 2.

3.1.5. Graded Terrain

[17] In addition to the flow-related landforms described here, there is a curious change in terrain texture proximal to the assemblage as a whole and to the valles in particular (Figure 10). Some portions of the surrounding intercrater plains material show a marked softening in topographic expression, with the characteristic hummocky texture grading evenly to smooth terrain with no clear boundary between the two (Figure 10, label 1). This grading is accompanied in places by linear topographic highs that resemble the furrows along broad channel floors (Figure 10, label 2). Some impact basins and craters within the intercrater plains material that do not form part of the contiguous smooth plains nonetheless appear to have been flooded to a variety of depths (Figure 10, label 3), though not all have breached perimeters.

3.1.6. Apparent Topographic Anomaly

[18] MLA gridded topography data [*Zuber et al.*, 2012] reveal the generally expected contrast in elevation between low-lying smooth plains material and adjacent higher standing intercrater plains units (Figure 11a). Flooded impact features greater than ~40 km in diameter retain a gently concave topography (Figure 11a, label 1), whereas those portions of the intercrater plains with textures grading from rough to smooth show a corresponding decrease in relative elevation (Figure 11a, label 2). We also note, however, an apparent topographic anomaly within at least two of the broad channels, Angkor and Timgad Valles (Figure 11a, label 3). Instead of a monotonically "downhill" profile, the cross-sections along both channels show a broad topographic rise several hundreds of kilometers in half-wavelength with a crest approximately midway along the channel (Figures 11b and 11c), as well as a number of shorter-wavelength variations in topography. On the basis of the gridded MLA DTM, the elevation range along Angkor Vallis is 426 m, and that along Timgad Vallis is 689 m. The topography of the entire study region is shown in Figure 12.

3.2. Flow Rate Analysis

[19] To calculate possible lava flow rates through a single broad channel, we applied a set of equations for confined flows, taken from *Williams et al.* [2001a], to calculate iteratively the Reynolds number (*Re*), friction coefficient (λ), and flow velocity (u) for two lava viscosities. These equations are useful for describing flow in a

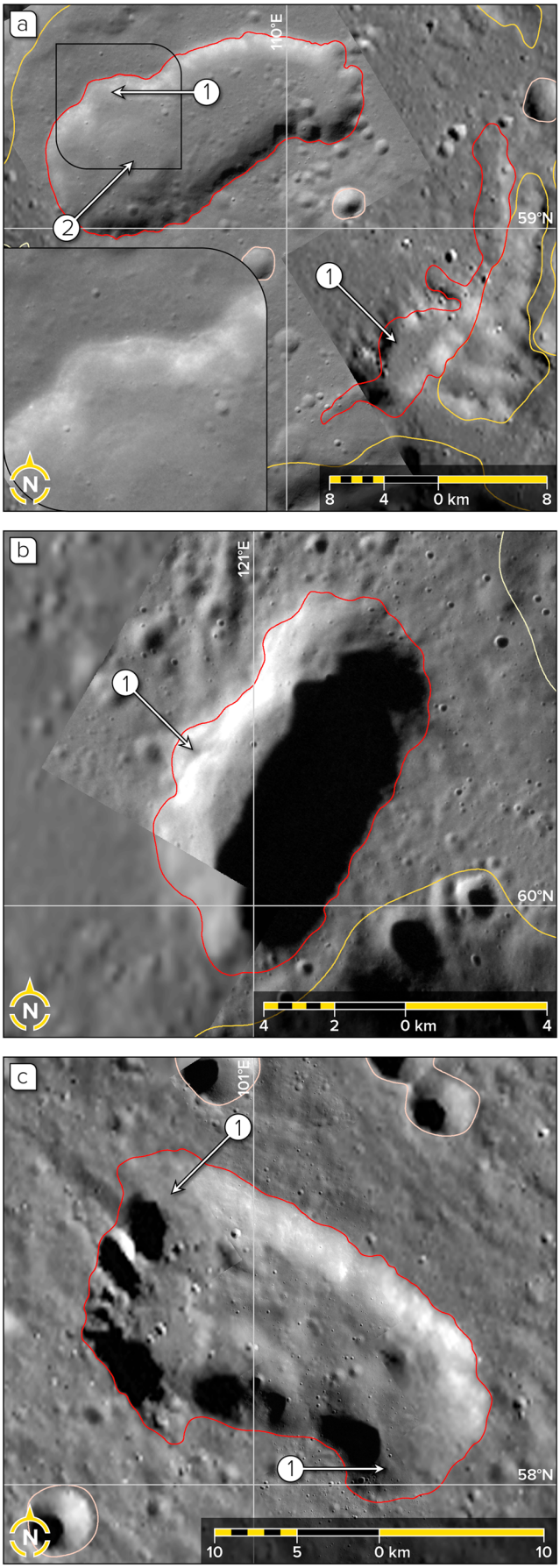

Figure 9.

non-circular lava channel having a width greater than its depth, such as the broad channels in our study area. We selected Angkor Vallis for our analysis, as it has well-defined margins and it adjoins the 136-km-diameter Kofi basin at its southeastern end. We treated the lava flow as turbulent on the basis of the lava surface morphologies described in section 3.1, though we acknowledge that this need not be the exclusive flow regime during lava emplacement. From each flow velocity and an estimate for the volume of volcanic fill within this basin, we determined the corresponding fill times.

[20] We calculated the flow velocity of turbulent lava in Angkor Vallis from the relation given by *Jarvis* [1995]:

$$u = \sqrt{\frac{4gh\sin(\psi)}{\lambda}}, \tag{1}$$

where g is the gravitational acceleration on Mercury's surface (in m s^{-2}), h is the lava flow thickness (in m), ψ is the channel slope (in degrees), and λ is the lava friction coefficient [*Kakaç et al.*, 1987]. This last parameter is defined as

$$\lambda = \frac{1}{[0.79\ln(Re) - 1.64]^2}. \tag{2}$$

[21] Here, Re is the Reynolds number for the flow system ($Re \gg 2000$ denotes a turbulent flow regime, which we considered appropriate for the lavas hosted within Angkor Vallis) and is given by [*Holman*, 1990]

$$Re = \frac{2\rho_b uh}{\mu_b} \tag{3}$$

where ρ_b denotes the lava bulk density (in kg m^{-3}), μ_b is the lava bulk dynamic viscosity (in Pa s), and u is the value for lava flow velocity (in m s^{1}) given by equation (1) (Table 3).

[22] The surface gravitational acceleration on Mercury is 3.7 m s^{-2}. As individual flow units within Angkor Vallis are not visible even in NAC images, and as there are no unambiguous high lava stand marks along the channel margins, lava flow thicknesses are unknown, and so we looked to corresponding measurements on other terrestrial planets for guidance in selecting appropriate values. Reported thicknesses for channelized basaltic flows on Hawaii are 1–10 m [*Griffiths*, 2000], with pahoehoe sheet flows on the flanks of Kilauea 1–5 m thick [*Hon et al.*, 1994]. Flows within the Imbrium basin on the Moon can have thicknesses of 10–30 m [*Zimbelman*, 1998], whereas those within other nearside basins have average thicknesses of ~30–60 m [*Hiesinger et al.*, 2002]. A lobate flow in the Sternia Fluctus area on Venus was inferred to have a

Figure 9. (a–c) Four coalesced depressions at three sites in our study area. Each depression is characterized by an irregular outline (label 1). The depression at the top left in (a) features a smaller, circular pit (label 2). Faint strata are visible in high-resolution images of its northern wall, though this layering is not apparent in NAC images of other depressions. Azimuthal equidistant projections, centered at (a) 59°N, 110°E, (b) 60°N, 121°E, and (c) 58.2°N, 101°E.

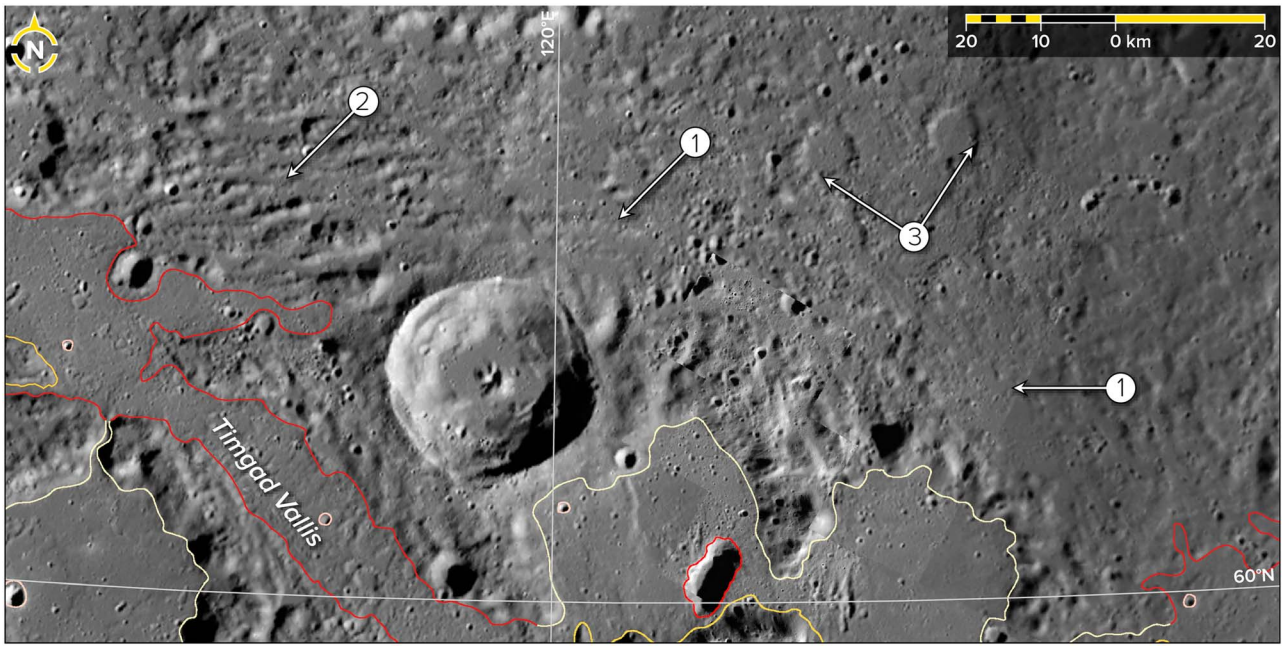

Figure 10. An example of an area where the intercrater plains material surrounding the channel assemblage displays a change in texture toward a more muted topographic expression (label 1). Furrows outside the assemblage resemble those on the broad channel floors (label 2); some small craters superposed on intercrater plains material appear partially flooded without being obviously connected to the contiguous smooth plains units (label 3). Azimuthal equidistant projection, centered at 60.8°N, 120.9°E.

Table 1. Morphometric Information for Broad and Narrow Channels

		Broad Channels				
		Latitude (°)[b]	Longitude (°)[b]	Length (km)	Width (km)[c]	Depth (m)[d]
	Angkor Vallis	57.96	113.25	86	28	400
	Cahokia Vallis	65.52	127.04	87	21	500
	Caral Vallis	62.76	128.84	54	19	400
	Paestum Vallis	60.28	126.12	102	21	300
	Timgad Vallis	60.89	116.6	140	12	600
		Narrow Channels				
Number	**Figure[a]**	**Latitude (°)[b]**	**Longitude (°)[b]**	**Length (km)**	**Width (km)[c]**	**Depth (m)[d]**
1	7a	61.86	104.29	61	7	150
2	7b	64.76	125.3	70	6	100
3	7b	63.54	125.27	161	3	180
4	7c	56.86	110.92	103	7	250
5	7d	56.78	124.18	44	9	160

[a]Figure indicates the panel in which the listed channel is shown in Figure 7.
[b]Latitude and longitude values are those of the centroid of each channel, calculated from its perimeter.
[c]Width values are averages of three measurements taken at an even spacing along the channel length.
[d]Depth values are averages of measured differences in elevation between the channel margin and channel floor at the locations where width values were determined.

Table 2. Morphometric Information for Coalesced Depressions

Number	Figure[a]	Latitude (°)[b]	Longitude (°)[b]	Long Axis (km)	Short Axis (km)	Depth (m)[c]
1	9a (top)	59.14	109.46	24	13	700
2	9a (bottom)	58.8	110.45	25	6	250
3	9b	60.09	121.04	12	6	200
4	9c	58.25	101.09	29	17	1100

[a]Figure indicates the panel in which the listed depression is shown in Figure 9.
[b]Latitude and longitude values are those of the centroid of each coalesced depression, as in Table 1.
[c]Depth values are averages of several measured differences in elevation between the depression rim and floor.

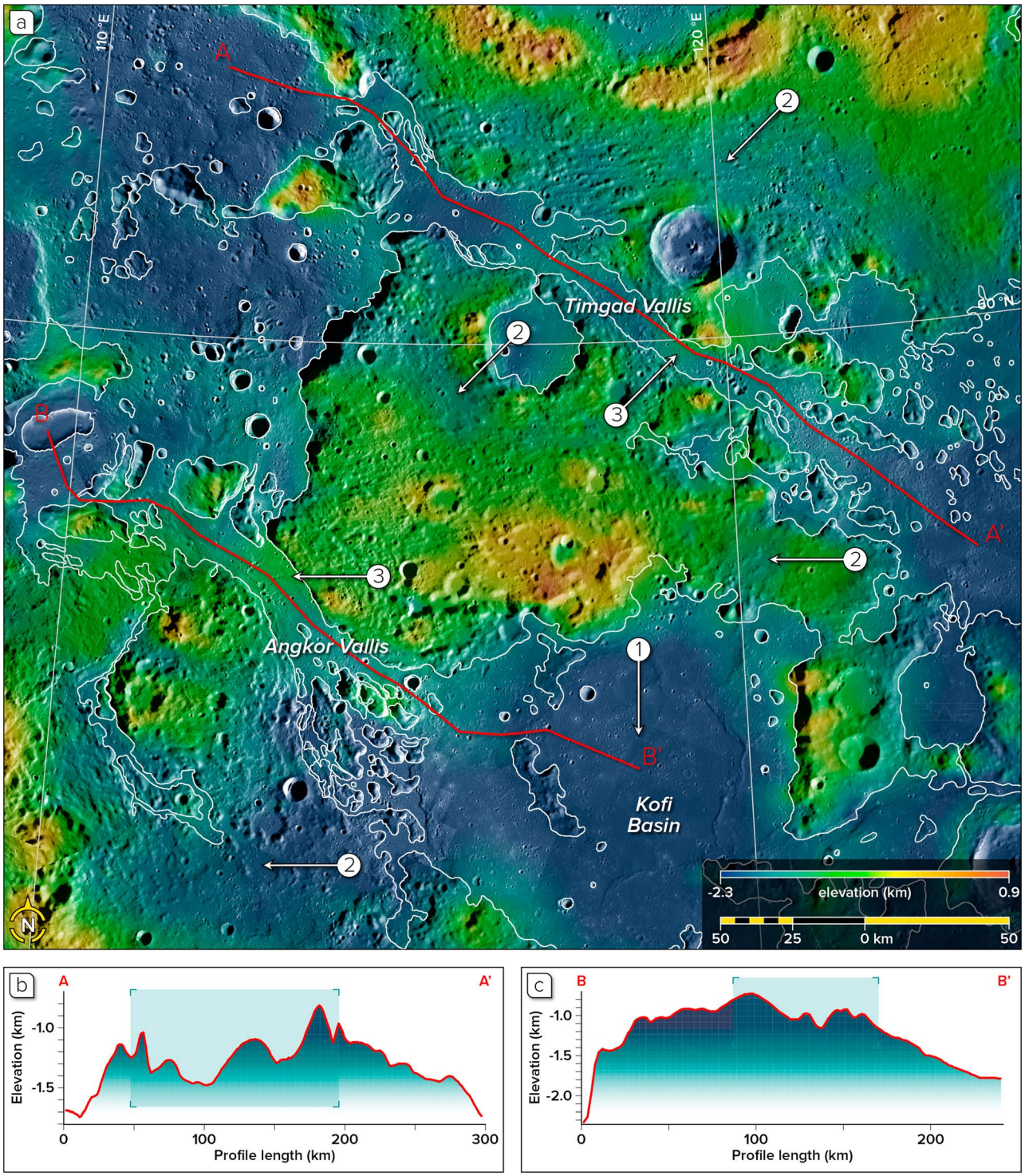

Figure 11. The topography of the northern flow-features assemblage. (a) A portion of a DTM derived from MLA profiles [*Zuber et al.*, 2012] overlaid on the MDIS monochrome base map from Figure 2. Blue colors correspond to lower elevations, and green through red colors denote higher-standing terrain. As in Figure 2, the area of contiguous smooth plains is outlined in white. Small variations in smooth plains topography include subtle concavities in flooded impact basins (label 1). Of note, those regions of intercrater plains material at elevations similar to smooth plains display muted textures (label 2), and both broad channels in this view, Angkor and Timgad Valles, have topographic profiles along their lengths characterized by broad rises rather than monotonically "downhill" gradients (label 3). Red lines indicate the locations of topographic profiles A–A′ and B–B′. Azimuthal equidistant projection, centered at 59°N, 116°E. (b) Topographic profile A–A′ along Timgad Vallis. (c) Topographic profile B–B′ along Angkor Vallis. For both profiles, the shaded region corresponds to the portion of the profile from which the elevation ranges given in section 3.1.6 were determined.

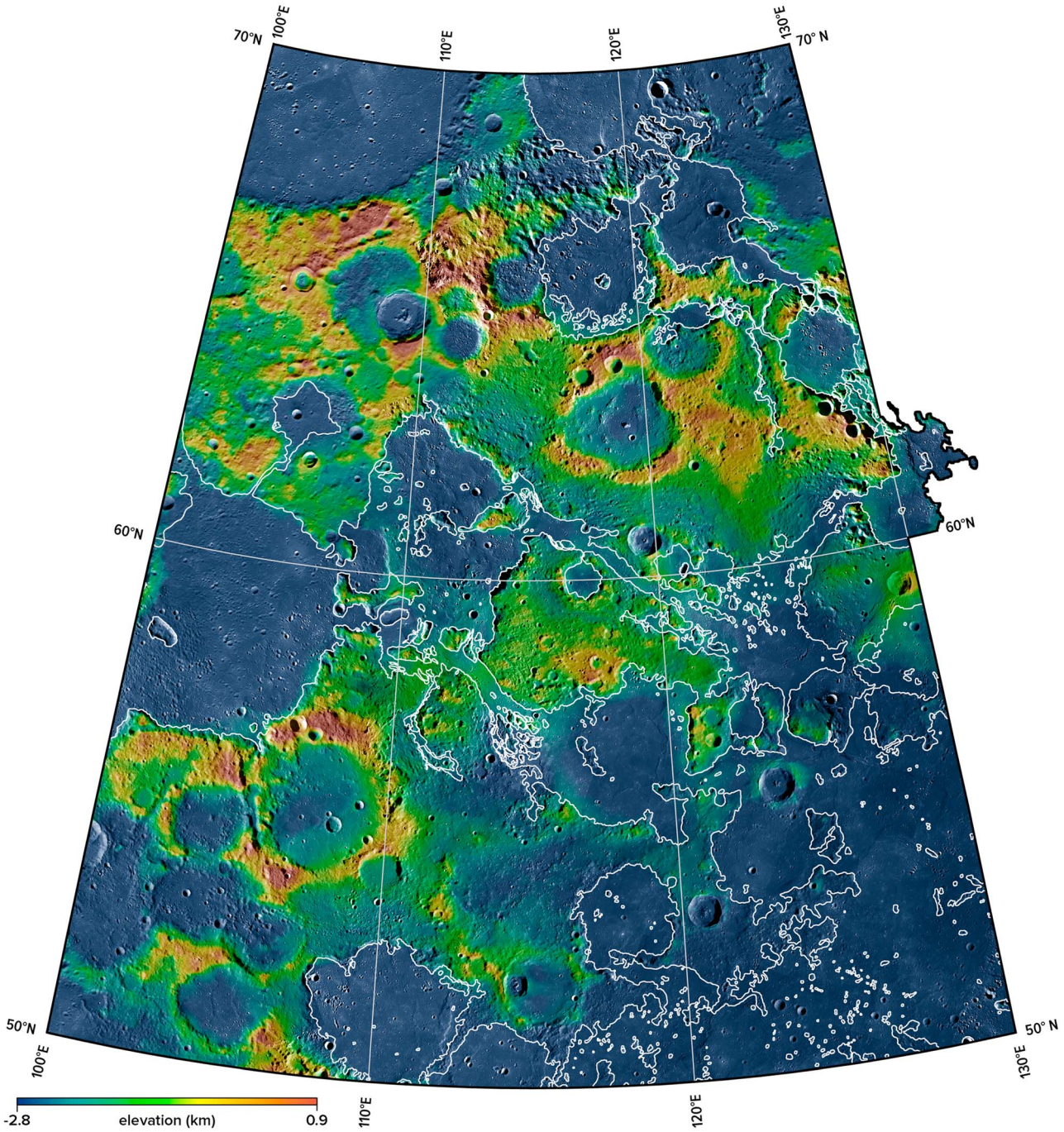

Figure 12. The topography of the entire study region, from a portion of a DTM derived from MLA profiles [*Zuber et al*., 2012] overlaid on the MDIS monochrome base map from Figure 2. The area of contiguous smooth plains is outlined in white.

thickness of some 30 m, whereas flows in the Tharsis region on Mars are 30–100 m thick [*Zimbelman*, 1998]. Possible ultramafic flows on Io have a thickness, estimated from shadow measurements, of ~8–10 m [*Williams et al*., 2001b]. Finally, although *Jaeger et al*. [2010] estimated an average thickness of 20 m for the Athabasca Valles flow unit, they suggested depths of up to 97 ± 10 m locally within the main channel. Therefore, we took values of 1, 10, and 100 m as a representative set of flow thicknesses within Angkor Vallis that likely span the actual value (Table 3).

[23] Another unknown is the channel slope, as this parameter changes along the length of Angkor Vallis (Figure 11c). Moreover, the unusual topography of the area indicates that the topography of the region has changed since the formation of Angkor Vallis and thus renders unreliable any attempts to estimate the original, unmodified channel slope. We therefore used slope values of 0.1°, 0.5°, and 1.0°, which are similar to values used in other studies of lava flow rates [e.g., *Williams et al*., 2001a; *Hurwitz et al*., 2013] (Table 3).

Table 3. Parameters and Results for Flow Analyses

Lava Composition	T (°)	ρ_b (kg m^{-3})	μ_b (Pa s)	g (m s^{-2})
Komatiite	1360[a]	2950	1.23[b]	3.71
ψ (°)	***h* (m)**	***Re***	**λ**	***u* (m s^{-1})**
0.1	1	3,800	0.04	0.8
0.5	1	9,700	0.03	2.0
1	1	14,500	0.03	3.0
0.1	10	195,000	0.02	4.1
0.5	10	473,000	0.01	9.9
1	10	693,000	0.01	14.4
0.1	100	8,490,000	<0.01	17.7
0.5	100	20,100,000	<0.01	41.9
1	100	28,600,000	<0.01	59.5
Tholeiite	1150[a]	2750	160[c]	3.71
ψ (°)	***h* (m)**	***Re***	**λ**	***u* (m s^{-1})**
0.1	1	19	0.09	0.5
0.5	1	52	0.06	1.5
1	1	79	0.05	2.3
0.1	10	595	0.09	1.7
0.5	10	1,650	0.06	4.8
1	10	2,500	0.05	7.3
0.1	100	36,800	0.02	10.7
0.5	100	91,200	0.02	26.5
1	100	134,000	0.02	39.1

[a]*Williams* [1998].
[b]*Ghiorso and Sack* [1995].
[c]*Williams and McBirney* [1979].

[24] As noted above, we calculated flow rates for two lava viscosities, selected on the basis of chemical remote sensing results from MESSENGER's X-Ray Spectrometer (XRS) instrument. XRS spectra indicate that Mercury's surface is relatively Mg rich, but Al, Ca, and Fe poor, compared with terrestrial and lunar basalts, indicative of a bulk surface composition intermediate between low-Fe basaltic and high-Mg ultramafic lithologies [*Nittler et al*., 2011]. More recent analysis has suggested a compositional difference between the northern smooth plains and the surrounding intercrater plains and heavily cratered terrain [*Stockstill-Cahill et al*., 2012; *Weider et al*., 2012]. We therefore considered two lava compositions, tholeiitic basaltic and komatiite, as representative end-members for the lavas in the study area. These compositional choices, and their corresponding eruptive temperatures, in turn informed the values of lava bulk density and dynamic viscosity used in our calculations (Table 3).

[25] Together with a length measurement for Angkor Vallis and an estimate for the volume of fill within Kofi basin, we used our derived lava flow velocities to calculate fill times for the basin (Table 4). We took the volume of fill within the Kofi basin calculated by *Hurwitz et al.* [2013] as this estimate. Their approach involved comparing the unfilled volume of Kofi with the volume of a similar sized basin with no volcanic fill, the 130-km-diameter Eminescu basin (centered at 10.7°N, 114.3°E) [*Schon et al*., 2011]. The difference between these volume measurements yields an estimate for the volume of fill within Kofi basin of 1.5×10^4 km^3 [*Hurwitz et al.*, 2013]. We discuss the results of our flow analysis, together with some limitations inherent to our approach, in section 4.2.

4. Discussion

4.1. Flow-Related Features

4.1.1. Broad Channels

[26] The five broad channels we have described here (Figure 5) are morphologically similar to wide outflow channel systems observed on Mars [e.g., *Baker and Kochel*, 1978] and Venus [e.g., *Head et al*., 1991] (though we note the absence of an equally wide lunar counterpart), which are characterized by low channel sinuosity, streamlined bedforms, terraced margins, and longitudinal grooves [*Baker and Kochel*, 1979; *Baker et al*., 1992; *Leverington*, 2007]. Early workers also drew comparisons between the examples on Mars and analogous features in the Channeled Scabland on Earth, which are thought to have formed during a rapid, voluminous discharge of water during the Pleistocene [*Baker and Milton*, 1974]. Martian outflow channels were thus assigned a diluvial origin due to the swift release of large volumes of groundwater [e.g., *Masursky et al*., 1977; *Coleman*, 2003; *Manga*, 2004].

[27] Liquid water is not stable at the surface temperature and pressure on Mercury, and so we discount an aqueous fluid as the responsible agent for the broad channels we observed. We also discount channel formation via erosion by impact melt, which would lack the necessary flux, volume, and spatial distribution required to form the expansive channel network seen on Mercury.

[28] Given the proximity of the outflow channels in our study to the northern volcanic plains and the circum-Caloris plains, we suggest that these features may have been produced, at least in part, by lava erosion. There is a large body of literature in which the erosive capacity of lava has been invoked as a mechanism for the formation of channelized landforms on terrestrial planets, including the Moon [e.g., *Greeley*, 1971; *Hulme*, 1973; *Williams et al*., 2000; *Hurwitz et al*., 2012], Venus [e.g., *Komatsu et al*., 1992, 1993], Mars [e.g., *Leverington*, 2004; *Williams et al*., 2005], and Io [*Williams et al*., 2001b; *Schenk and Williams*, 2004]. Such lava erosion would have led to streamlined erosional residuals, to which the elongate kipukas in Mercury's valles may correspond. Lava erosion is accomplished via a combination of thermal and mechanical processes, with the capacity of lava to incise through substrata enhanced by factors such as higher temperatures, lower viscosity, and more turbulent flow conditions [e.g., *Leverington*, 2007; *Hurwitz et al*., 2012].

Table 4. Angkor Vallis Flow Rates and Fill Times for Kofi Basin

Komatiite (1360 °C)					
ψ (°)	***h* (m)**	***u* (m s^{-1})**	***Q* (m^3 s^{-1})**	T_{Fill} **(s)**	T_{Fill} **(days)**
0.1	1	0.8	2.2×10^4	6.8×10^8	7890
0.5	1	2.0	5.6×10^4	2.7×10^8	3100
1	1	3.0	8.4×10^4	1.8×10^8	2100
0.1	10	4.1	1.1×10^6	1.4×10^7	158
0.5	10	9.9	2.8×10^6	5.4×10^6	62
1	10	14.4	4.0×10^6	3.8×10^6	43
0.1	100	17.7	5.0×10^7	3.0×10^5	3
0.5	100	41.9	1.2×10^8	1.3×10^5	1
1	100	59.5	1.7×10^8	8.9×10^4	<1
Tholeiite (1150 °C)					
ψ (°)	***h* (m)**	***u* (m s^{-1})**	***Q* (m^3 s^{-1})**	T_{Fill} **(s)**	T_{Fill} **(days)**
0.1	1	0.5	1.4×10^4	1.1×10^9	12,400
0.5	1	1.5	4.2×10^4	3.6×10^8	4,130
1	1	2.3	6.4×10^4	2.3×10^8	2,700
0.1	10	1.7	4.8×10^5	3.1×10^7	362
0.5	10	4.8	1.3×10^6	1.2×10^7	134
1	10	7.3	2.0×10^6	7.5×10^6	87
0.1	100	10.7	3.0×10^7	5.0×10^5	6
0.5	100	26.5	7.4×10^7	2.0×10^5	2
1	100	39.1	1.1×10^8	1.4×10^5	<2

[29] There is strong geochemical evidence that much of Mercury's crust is mafic to ultramafic in composition [*Nittler et al*., 2011; *Stockstill-Cahill et al*., 2012; *Weider et al*., 2012] (see section 3.2). The low SiO_2 content, high liquidus temperatures, and high densities of these lithologies when molten, relative to more evolved melts, means that the factors listed above will be all the more relevant, especially for ultramafic, komatiite-like compositions. Taken together, therefore, the morphological observations we document and the geochemical results reported by others provide a compelling case for the above-ground movement of, and mechanical and/or thermal erosion by, voluminous, high-temperature, low-viscosity mafic to ultramafic lavas.

[30] Lavas mechanically erode substrata by physically degrading and removing material, whereas thermal erosion is accomplished by the ablation and melting of country rock [e.g., *Williams et al*., 2001a; *Leverington*, 2007]. Consolidated substrata, such as solidified basalts, resist mechanical erosion to a greater extent than less cohesive material (e.g., impact regolith), whereas hotter surfaces are thermally eroded in less time than that required for cooler material [*Hurwitz et al*., 2010]. *Hurwitz et al*., [2013] calculated and discussed possible erosion rates for Angkor Vallis, on the assumption that the channel depth observed today represents the maximum extent of incision. They concluded that thermal erosion was likely the dominant regime in which it formed, with the time taken to incise the channel differing by an order of magnitude (30–300 days) depending on the lava viscosity and channel slope (see their Table 3). (These workers also suggested that mechanical erosion may have contributed to initial channel formation in locations where unconsolidated substrata were present; although the depth of regolith is unknown and undoubtedly varies across the area, the round, softened forms of both channel kipukas and the margins of the coalesced depressions attest to at least some depth of surficial, loosely consolidated material.)

[31] Of course, the ability of lava to shape Mercury's broad channels would have been augmented by the presence of any preexisting linear depressions. *Fassett et al*. [2009] described a set of troughs and grooves radial to the Caloris basin within the geological unit termed the Van Eyck Formation [*McCauley et al*., 1981], which is regarded as terrain sculpted by the Caloris basin impact on the basis of similarity to terrain around large lunar basins. Of the broad channels we describe in this paper, all are part of the Van Eyck Formation, and all but one (Paestum Vallis) are radial to Caloris; indeed, two are featured in the study by *Fassett et al*. [2009] (Angkor and Timgad Valles, though the valles were not named as such at the time; see their Figure 7a).

[32] These observations, then, provide support for the formation of the broad channels by lavas that first flooded, and then modified the shape of, preexisting topographic depressions. Other radial troughs in the Van Eyck Formation of similar lengths and distances to Caloris feature scalloped margins in contrast to the regular edges of the broad channels, and they are not smooth floored, do not feature elongate kipukas aligned parallel to the trough axes, and do not form an interconnected network of smooth plains. Therefore, although we attribute the morphological characteristics of these channels to erosion by lava, the dimensions of preexisting impact-sculpted troughs and grooves likely played a controlling role in final channel morphometry in at least four cases.

[33] Definitive channel depths are difficult to estimate. The depths we quote in Table 1 are valid as absolutes only if total drainage of lavas within the valles occurred. Otherwise, the channel floors we observe represent the upper surfaces of cooling crusts formed by lavas that continued to flow at depth, potentially for some time. It is not possible to determine with certainty whether or not the channels were entirely drained (though the lack of benches along the channel walls suggests not), or to evaluate the initial depths of the precursory impact-sculpted troughs. We note, however, that a 15-km-wide trough to the northeast of Caloris (located at 41°N, 185°E), within the Van Eyck Formation but largely unfilled by Caloris exterior plains, has an approximate depth of ~2 km, substantially deeper than the depths for the valles we report in Table 1 and suggestive of a considerably greater depth than appears today.

[34] The majority of kipukas in our study area (Figure 6) are likely due to impact processes, reflecting portions of central peaks, peak rings, crater rims, and ejecta partially buried by volcanism, and this partial burial applies equally to kipukas within the channels, as remnants of original sculpted terrain. Streamlined forms within Martian outflow channels are often teardrop shaped, the result of hydraulic modification of obstacles in the channels that divert the flow, with the tapered point indicating the downstream direction [e.g., *Baker and Milton*, 1974; *Melosh*, 2011]. The examples within Mercury's broad channels are not characteristically teardrop in planform and so do not unequivocally indicate the flow direction within each channel. The flow direction instead is given, to within a 180° ambiguity, by the long axes of the channels themselves. Selecting between the two possible directions of flow through the valles is challenging, given that expansive (and possible source) regions of smooth plains are present both to the northwest and southeast of the flow assemblage. The splay-like pattern of kipukas at the southeastern end of Angkor Vallis (described in section 3.1.1) could represent a widening of the channel as lava encountered and flowed around a topographic barrier in the form of the Kofi basin rim, an interpretation that invokes a flow direction from northwest to southeast. We acknowledge that without clear flow indicators, however, this interpretation remains tentative.

[35] Finally, it is worth comparing the morphology and spatial locations of outflow channels on other bodies with those on Mercury. Broad channels on the innermost planet are not as well preserved as their counterparts on Mars and Venus, which may be the result of a higher impact flux on Mercury than those on other terrestrial planets [e.g., *Cintala*, 1992]. Venusian outflow channels can originate in large topographic depressions [*Baker et al*., 1992], and Martian channels often head in chaotic terrain [*Leverington*, 2009]. Few candidate source depressions are evident for Mercury's broad channels, but as each channel links flooded craters we cannot discount the possibility that distinct, early source vents were subsequently buried. Large channels on Mars and Venus also commonly exhibit complex patterns of braided and anastomosing reaches [*Masursky*, 1973; *Komatsu et al*., 1993], landforms that are largely absent from the valles we describe. In fluvial systems on Earth, such patterns arise from local increases in river slope or discharge [*Schumm*, 1985]; if such a relation is applicable to the channels on Mercury, we might infer that their slopes and discharges remained generally steady throughout their formation.

4.1.2. Narrow Channels

[36] The five narrow channels we describe (Figure 7) are morphologically similar to sinuous rilles documented on the Moon [e.g., *Hurwitz et al*., 2012] and Mars [e.g., *Byrne et al*., 2012a], as well as the "canali" on Venus [e.g. *Komatsu et al*., 1992, 1993]. Though there is some debate as to the fluid agent responsible for Martian rille formation [*Bleacher et al*., 2010; *Murray et al*., 2010], several workers concluded that sinuous rilles on the Moon formed by thermal erosion of the surface by high-effusion-rate lava flows [*Hulme*, 1973; *Mouginis-Mark et al*., 2008; *Williams et al*., 2000; *Hurwitz et al*., 2012], with pooling and subsequent drainage of lava a contributing factor, at least in the case of Vallis Schroteri [*Garry and Bleacher*, 2011]. More exotic compositions have been suggested as responsible for Venusian canali [e.g., *Baker et al*., 1992]. Therefore, a volcanological origin for the narrow channels on Mercury is not only plausible but consistent with their geological context and with analogous features elsewhere.

[37] No distinct source areas for these channels are evident. Three narrow channels link flooded craters and so do not have defined points of origin; the two examples that join the flow assemblage at one end show no depressions at their other, poorly defined ends that would correspond to source vents. In the absence of local vents, then, the narrow channels may have been formed by small pulses of lava that escaped the confines of broad channels and impact craters and that flowed in the downhill direction through lows in the intercrater plains, in some cases entering neighboring craters and helping to fill them, and in at least two instances extending some distance outside the main assemblage. Indeed, as these two channels do not have specific ends but instead appear to fade into muted portions of the surrounding plains, they may have helped to facilitate flooding of these plains by channeling of lavas flowing through the main flow feature assemblage.

[38] Should the streamlined kipukas within narrow channels represent erosional residuals, however, as they do in the broad channels, lava erosion may have also shaped these channels. The general morphometry of the narrow channels differs from those of the broad channels (Table 1), which may reflect different starting conditions. In the absence of preexisting linear depressions, such as those of impact origin we infer for the broad channels, and with no evidence of any tectonic landform having controlled the course of the narrow channels we describe, erosion of substrata by flows channelized by the hummocky intercrater plains could have exacerbated narrow channel formation. On the basis of analysis of similar channels elsewhere on Mercury, this erosion would likely have been almost entirely thermal in nature [*Hurwitz et al*., 2013].

4.1.3. Flooded Impact Features

[39] Those craters and basins that form part of the interconnected channel network (Figure 8) feature one or more breaches of their perimeters, through which lava entered before ponding. Flows would have exploited and widened existing gaps in basin and crater rims, or forced already weakened portions of rim walls to yield, or both. Some craters may have been flooded, either partially or completely, from flows entering at one point, before suffering a further breach in their perimeter elsewhere and so facilitating the onward flow of lava. Depending on the depth of volcanic infill within a given crater, impact-related structures such as central peaks or peak rings may have been partially or completely buried.

[40] The wrinkle ridges present within many flooded basins are similar to those distributed across the northern and other smooth plains regions on Mercury [*Strom et al*., 1975; *Head et al*., 2011], which formed due to shortening of surface units through folding above a blind reverse fault [e.g., *Watters*, 1988]. The ridges in our study area probably reflect a combination of global stresses imparted by the contraction of Mercury as its interior cooled [cf., *Hauck et al*., 2004] and basin-localized compression in response to volcanic-fill-induced subsidence [*Watters et al*., 2012], with local processes contributing to the orientation of those structures with basin-circumferential orientations.

4.1.4. Coalesced Depressions

[41] On the basis of their irregular, non-circular outlines, together with the lack of prominent raised rims about their perimeters, we discount an impact origin for the four depressions we have described (Figure 9). Instead, their locations within smooth plains units and their proximity to the channel landforms are consistent with a volcanic origin.

[42] Some depressions elsewhere on Mercury have been identified as sites of pyroclastic activity, on the basis of morphological and spectral characteristics. These vents often show evidence of coalescence; are located atop low, broad rises; and feature a halo of high-reflectance material that has a distinctively steeper or "redder" spectral slope over visible to near-infrared wavelengths than is typical for Mercury [*Kerber et al*., 2009, 2011]. Whereas the depressions in our study area have scalloped outlines (and thus probably experienced coalescence), there is no attendant rise, bright halo, or spectral contrast between the depression and its surroundings. If the features we describe here were source vents, any erupted material was likely not pyroclastic in nature, but effusive.

[43] Even so, there is no obvious morphological evidence for associated lava flows, by way of leveed margins, partially collapsed lava tubes, or chains of rootless vents characteristic of effusive volcanism [cf. *Bleacher et al*., 2007], even in targeted MDIS NAC data, so alternative interpretations for these landforms must be considered. The presence of a smaller, circular pit within the large depression to the northwest in Figure 8a resembles nesting of calderas as is observed on Mars, for example, within the summit caldera complexes of the Tharsis Montes [e.g., *Byrne et al*., 2012a]. No associated structural evidence of caldera collapse, e.g., a peripheral fault zone, is observed around this or any other depression, though such coherent structures need not necessarily form to facilitate the collapse of overlying strata into subsurface voids. Should these depressions correspond to magma chambers, however, it is unlikely that they alone hosted the volume of material that fed the voluminous flows in this region.

[44] Alternatively, the depressions may originally have been overlapping impact craters that were then filled by flows, serving to pond lava that eventually drained through subsurface lava tubes. Their crater rims could have been erased by the sustained flow of lavas, though it is not obvious why so few such depressions occur in a region replete with impact features. A final possibility is that these features correspond to lava rise pits (depressions formed by the inflation of a lava flow around an area that experienced little to no inflation [*Walker*, 1991]),

though their size, orders of magnitude larger than those on Earth, may preclude this interpretation.

[45] In any case, the lack of any apparent lava flows emanating from the depressions suggests collapse without related surface volcanism [e.g., *Walker*, 1975]. Seven other depressions outside our study area, each located within one of five impact craters or basins, were described by *Gillis-Davis et al*. [2009]. Termed "pit craters," these landforms have attributes similar to the depressions we describe: they are irregularly shaped, have no observable ejecta, and are rimless with steep sides. Pit craters also have dimensions similar to those we report in Table 2 (see Table 1 in *Gillis-Davis et al*. [2009]). These authors interpreted the pit craters as the result of collapse into underlying drained magma chambers.

[46] Under a scenario by which the depressions of this study formed by the lateral withdrawal of magma from shallow magma chambers through subsurface lava tubes, then, their flat floors formed by the infill of country rock that slumped into the pits after the evacuation of the tubes (such that the depressions are essentially very large collapse pits or calderas), with this slumping contributing to the formation of their scalloped margins. The faint fluting along the perimeter of the northwest depression in Figure 8a may correspond to small-scale failure of an upper stratum of poorly consolidated regolith. This scenario renders the depressions late-stage features that formed after surface flow within the channels had ceased, accounting for why they remain visible today and were not buried by subsequent lavas.

4.1.5. Graded Terrain

[47] The even grading of the intercrater plains material from its characteristic hummocky texture to a more muted surface expression (Figure 10) implies covering to some depth by volcanic material, with this depth a function of flow volume and preexisting topography. MLA gridded data show that the intercrater plains have local, shallow gradients today (Figures 11 and 12), and so it is possible that at least some of their lower-lying portions were inundated by lavas during channel formation, and the degree of surface tempering would correlate directly with the depth of cover.

[48] Under this interpretation, then, the inundation of the surrounding plains implies that at least some volume of eruptive materials was not constrained to the channels (broad or narrow), but instead flowed overland in a flood lava mode, perhaps reflecting temporary increases in eruptive flux. Such widespread inundation agrees with the interpretation of *Head et al*. [2011] for the emplacement of the northern plains as a whole. Impact basins and craters within the intercrater plains would have been filled through breaches in their perimeters by sheets of lava without the development of a channel network, but without a sufficient eruptive volume to bury these features entirely. (We regard the smooth deposits within craters that clearly postdate volcanic activity in this area as likely to be ponded impact melt, on the basis of the intact rims and relatively fresh appearances of these features.) As short-lived increases in eruptive flux waned, the flood-mode emplacement of lavas would have ceased, with lava drain-back serving to channelize these flows once more (similar to the scenario suggested by *Jaeger et al*. [2010] for flows within the Athabasca Valles outflow channel system on Mars).

[49] The linear patterns visible in parts of the graded terrain are consistent with this interpretation of erosion by flood mode lavas, via the removal of some small mounds and knolls, and the aggradation of lava behind other such features, resulting in ridges and furrows that partially channelized (and therefore indicate the direction of) the overland flows. The furrows occur close to the margins of the valles but then disappear, a pattern that might reflect a reduction in the erosive capacity of the lavas as they moved progressively beyond the confines of these channels.

4.1.6. Apparent Topographic Anomaly

[50] The general bimodal distribution of elevations in our study area, with channels and flooded craters occupying lower elevations than those of the surrounding intercrater plains material, supports our interpretation that lavas flooded and shaped, through mechanical and/or thermal erosion, existing depressions (impact craters and impact-sculpted terrain). That those portions of intercrater plains with muted textures are also low-lying, and so would have been susceptible to inundation by lavas not constrained by the channels, bolsters this interpretation.

[51] However, the topographic rises along Angkor and Timgad Valles shown in Figure 11 are not an anticipated consequence of surface lava flow. A constructional component to relief within lava channels has been reported on Earth, in situations where solidified crust accumulates at sites of channel constriction [*Lipman and Banks*, 1987; *Bailey et al*., 2006] even as a consistently downhill gradient beneath the crust ensures that flow continues. Such constrictions are often temporary, however, removed by continued flow of lava from upstream, and are usually at the meter scale. Although the channels on Mercury may narrow somewhat at the locations where the rises appear to crest, they are still on the order of 10 km wide at these points. Local reverse gradients have been observed in outflow channels elsewhere (e.g., along the course of Kasei Valles [*Robinson and Tanaka*, 1990]), and the amplitudes of the rises we show here are substantially less than their wavelengths (the aspect ratio of the largest amplitude rise in the Figure 11b profile corresponds to an uphill grade of 1:40). Nonetheless, such a gradient would have presented a substantial impediment to the uphill flow of even high volumes of low-viscosity lavas.

[52] There is a growing catalog of topographic anomalies on Mercury that attest to long-wavelength changes in topography since the end of the Late Heavy Bombardment ~3.8 Ga [*Solomon et al*., 2012]. The northern and southern portions of the 1640-km-diameter Caloris basin floor are elevated, in some parts to levels above the basin rim, and an east–west-oriented trough crosses its center [*Oberst et al*., 2010; *Preusker et al*., 2011; *Zuber et al*., 2012]. This long-wavelength topography does not appear to be the result of volcanic construction, and it shows no evidence of control by the myriad tectonic structures within the basin [*Byrne et al*., 2012b]. A broad region some 1000 km across in Mercury's smooth northern plains rises ~1.5 km above the surrounding terrain and includes on its flanks craters flooded by plains units whose floors are tilted away from the rise center at angles similar to those of the flank slopes themselves [*Klimczak et al*., 2012; *Zuber et al*., 2012]. Such tilted craters strongly suggest that uplift of the rise occurred after plains emplacement. Finally, extensive contractional tectonic systems that bound regions of high-standing terrain on Mercury show evidence of a contribution to long-wavelength topographic relief at a scale of several

hundred kilometers, on the basis of tilted crater floors proximal to these systems [*Byrne et al*., 2012c].

[53] Several candidate mechanisms for such deformation have been suggested. In some models of mantle convection in Mercury's comparatively thin mantle (relative to the other terrestrial planets), for instance, dynamic topography is predicted to display amplitudes and wavelengths similar to the observations described above [*King*, 2008]. Lithospheric folding, in response to horizontal shortening driven by global contraction, might also account for at least some measure of topographic change on Mercury [*Dombard et al*., 2001]. Although the shortest of the wavelengths of the topographic variations in the channels, at several tens of kilometers, are substantially shorter than those documented elsewhere or predicted by earlier studies, the longest-wavelength variations along the two valles are at a comparable scale.

4.2. Flow Analysis

[54] The results of our flow analysis for Angkor Vallis are given in Table 3, with calculated values for Reynolds number, *Re*, lava friction coefficient, λ, and flow velocity, *u*, tabulated with corresponding values for slope, ψ, and flow thickness, *h*. We found that *u* for parameters appropriate to komatiite lava at 1360 °C range from $<1\,m\,s^{-1}$ to almost $60\,m\,s^{-1}$ and depend on flow thickness and slope, whereas tholeiitic basalt at 1150 °C with the same range of thickness and slope had velocities of between 0.5 and $39\,m\,s^{-1}$. These end-member values likely bracket the actual span of flow velocities for the channelized flows described here; some combinations of flow thickness and channel floor slope yield values of *u* comparable to flows on Earth (e.g., the 1801 Kaupulehu lava flow of Hualalai volcano reported by *Baloga et al*. [1995]) and those within Athabasca Valles [*Jaeger et al*., 2010]. Of nine sets of variables for komatiite lava, all yielded derived values for *Re* in excess of 2000, the threshold above which flows are considered to be turbulent, whereas only five of nine variable sets for tholeiite lava satisfied this condition for turbulent flow. Should the lava morphologies we describe be the result of turbulent flow (see section 3.2), those *Re* values less than 2000 may not correspond to probable flow thicknesses and channel floor slopes.

[55] Calculated values for lava flow rate, *Q*, lie between 2.2×10^4 and $1.7 \times 10^8\,m^3\,s^{-1}$ for komatiite, and between 1.4×10^4 and $1.1 \times 10^8\,m^3\,s^{-1}$ for tholeiite. If the estimated flow rates for these lavas are representative of their effusion rates, then the lower *Q* values correspond to effusion rates only an order of magnitude greater than those postulated for historic, large-volume eruptions on Earth, as well as those for large lava flows on Mars [e.g., *Baloga and Glaze*, 2008; *Glaze et al*., 2009]. Moreover, the highest *Q* value we calculate ($1.7 \times 10^8\,m^3\,s^{-1}$) is within the effusion rate limit for hypothesized large dikes thought to underlie major graben systems on Mars, e.g., Cerberus Fossae [*Jaeger et al*., 2010].

[56] From our calculated *u* and *Q* values, cross-sectional areas of 0.028, 0.28, and $2.8\,km^2$ for Angkor Vallis (see Tables 1 and 3), and the estimated fill volume in Kofi basin of $1.5 \times 10^4\,km^3$, komatiitic lavas would have taken between 22 years and ~1 day to fill the basin, depending on slope and flow thickness. Corresponding fill times for tholeiitic basaltic lavas range from 34 years to less than 2 days (Table 4). These are end-member values. A 1-m-thick komatiite flow would solidify long before filling Kofi basin, whereas a fill time of less than 2 days requires the rapid evacuation from depth of enormous volumes of lava. However, a tholeiitic flow 100 m thick, or a 10-m-thick komatiite, would fill Kofi basin in months (with thicker komatiite flows reducing that time to several tens of days). These latter fill times are in line with the thermal erosion rates calculated by *Hurwitz et al.* [2013] in their study of the formation of this same broad channel (see section 4.1.1).

[57] It should be stressed that our analysis has inherent limitations. For instance, the channel cross-sectional areas we used are functions of assumed flow thickness (for a fixed channel width). These figures may not reflect Angkor Vallis' original carrying capacity and may thus over-represent actual fill times if that capacity were greater. Moreover, our analysis considers only one broad channel out of a population of five. If each channel were shaped during the same eruptive event, then the effusion rate from the presumably now-buried source(s) of lava would have been substantially higher than that suggested by the flow rates calculated for this individual vallis. Nonetheless, the mid-range fill times we report are consistent with those of *Head et al*. [2011], who concluded, on the basis of geological and geochemical observations, that the lavas responsible for the northern plains were emplaced rapidly, relative to more typical eruptions on other inner planets, and in large volumes, the result of extensive partial melting of Mercury's mantle and ensuing high effusion rates and widespread volcanism in a flood lava mode.

5. Concluding Remarks

[58] We have documented an assemblage of flow-related landforms in Mercury's northern hemisphere, including broad and narrow channels, coalesced depressions that may correspond to calderas, and evidence of partial resurfacing by lavas of adjacent intercrater plains. We interpret this assemblage as having formed by the channelized flow of voluminous, high-temperature, low-viscosity lavas of mafic to ultramafic composition, under a scenario whereby lavas coursed through existing impact-sculpted and impact-cratered terrain, producing an interconnected network of smooth plains characterized by flooded impact craters linked by broad channels. Periods of increased eruptive flux may have produced pulses of lava that exceeded the carrying capacity of the channels, resulting in the emplacement of flows outside the channels in a flood lava mode that partially inundated the surrounding plains. A first-order flow analysis shows that for plausible input parameters, lava flow rates were high and fill times of a basin in our study area were short, on the order of several months to tens of days. Large-scale processes later modified the long-wavelength topographic signature of the area.

[59] The presence of the flow feature assemblage so close to the vast northern plains, together with tentative evidence of channelized flows originating from the direction of these plains (see section 4.1.1), raises the prospect that the flow assemblage and the northern plains might be temporally related. Such a relationship leads to an intriguing possibility. The evidence for inundation of plains surrounding the flow

features that we document here attests to some measure of overland flood volcanism, like that suggested for the northern plains, but of insufficient volume for complete burial. As flood volcanism is likely to be supply limited (rather than cooling limited) [e.g., *Head et al*., 2012], the lavas that shaped the flow assemblage could have been emplaced toward the end, and so reflect the waning supply, of an eruptive event—perhaps that responsible for the northern plains. If so, then the flow features we report are distinctive on Mercury only in that they are preserved today. Similar features may have commonly prefaced total burial by smooth plains emplaced in an impact-sculpted and impact-cratered region, but for most such features no evidence remains after flood emplacement was complete.

[60] Finally, there has been debate as to whether lavas can be emplaced turbulently in a single flood event [e.g., *Reidel and Fecht*, 1987], or if flood basalts instead form by the long-term inflation of sequentially emplaced flows [e.g., *Hon et al*., 1994; *Self et al*., 1998]. Our observations cannot substantially add to this debate, for even with targeted NAC images we could not identify individual lava flows or other morphological features such as tumuli, lava rises, and lava rise pits [*Walker*, 1991] that characterize and so might help determine the likelihood of lava flow inflation.

[61] However, the channelized landforms in the northern flow assemblage are morphologically similar to landforms on other planets for which turbulent lava flow has been invoked as the formative mechanism. Recent high-resolution observations of the Athabasca Valles outflow channel system on Mars [*Jaeger et al*., 2010] indicate that the associated flood-lava flows, which cover some 250,000 km^2, were emplaced turbulently in a single eruptive event over a period lasting no more than several weeks. Our findings support the notion that lavas can at least contribute to the formation of outflow channels on other planets, so that those on Mars need not exclusively be the product of catastrophic flood waters but can also reflect a volcanological signature. The formation on Mercury of such channels and related landforms by turbulent lava therefore not only has geological precedent, but such a genesis may be characteristic of large igneous provinces in general.

[62] **Acknowledgments.** We thank Christopher Hamilton (NASA Goddard Space Flight Center) and Karl Mitchell (Jet Propulsion Laboratory) for constructive discussion during the preparation of this manuscript. Jacob Bleacher and Lori Glaze (both at NASA Goddard) are also thanked for thoughtful reviews that markedly improved this manuscript. The MESSENGER project is supported by the NASA Discovery Program under contracts NASW-00002 to the Carnegie Institution of Washington and NAS5-97271 to The Johns Hopkins University Applied Physics Laboratory. This research has made use of NASA's Astrophysics Data System.

References

Bailey, J. E., A. J. Harris, J. Dehn, S. Calvari, and S. K. Rowland (2006), The changing morphology of an open lava channel on Mt. Etna, *Bull. Volcanol.*, *68*, 497–515.

Baker, V. R., and D. J. Milton (1974), Erosion by catastrophic floods on Mars and Earth, *Icarus*, *23*, 27–41.

Baker, V. R., and R. C. Kochel (1978), Morphometry of streamlined forms in terrestrial and martian channels, *Proc. Lunar Planet. Sci. Conf*., *9th*, 3193–3203.

Baker, V. R., and R. C. Kochel (1979), Martian channel morphology: Maja and Kasei Valles, *J. Geophys. Res.*, *84*, 7961–7983.

Baker, V. R., G. Komatsu, T. J. Parker, V. C. Gulick, J. S. Kargel, and J. S. Lewis (1992), Channels and valleys on Venus: Preliminary analysis of Magellan data, *J. Geophys. Res.*, *97*, 13,421–13,444.

Baker, D. M. H., J. W. Head, S. C. Schon, C. M. Ernst, L. M. Prockter, S. L. Murchie, B. W. Denevi, S. C. Solomon, and R. G. Strom (2011), The transition from complex crater to peak-ring basin on Mercury: New observations from MESSENGER flyby data and constraints on basin formation models, *Planet. Space Sci.*, *15*, 1932–1948, doi:10.1016/j.pss.2011.05.010.

Baloga, S. M., and L. S. Glaze (2008), Self-replication model for long channelized lava flows on the Mars plains, *J. Geophys. Res.*, *113*, E05003, doi:10.1029/2007JE002954.

Baloga, S. M., P. D. Spudis, and J. E. Guest (1995), The dynamics of rapidly emplaced terrestrial lava flows and implications for planetary volcanism, *J. Geophys. Res.*, *100*, 24,509–24,519.

Becker, K. J., L. A. Weller, K. L. Edmunsdson, T. L. Becker, M. S. Robinson, A. C. Enns, and S. C. Solomon (2012), Global controlled mosaic of Mercury from MESSENGER orbital images, *Lunar Planet. Sci.*, *43*, abstract 2654.

Bleacher, J. E., R. Greeley, D. A. Williams, S. R. Cave, and G. Neukum (2007), Trends in effusive style at the Tharsis Montes, Mars, and implications for the development of the Tharsis province, *J. Geophys. Res.*, *112*, E09005, doi:10.1029/2006JE002873.

Bleacher, J. E., A. P. de Wet, W. B. Garry, J. R. Zimbelman, and M. E. Trumble (2010), Volcanic or fluvial: Comparison of an Ascraeus Mons, Mars, braided and sinuous channel with features of the 1859 Mauna Loa flow and Mare Imbrium flows, *Lunar Planet. Sci.*, *41*, abstract 1612.

Byrne, P. K., C. Klimczak, B. W. Denevi, T. R. Watters, S. C. Solomon, A. C. Enns, J. W. Head, D. M. Hurwitz, and D. M. Baker (2011), Surface lava flow features on Mercury, *Abstracts with Programs*, *43*, paper 142-7, p. 358, Geological Society of America, Boulder, Colo.

Byrne, P. K., B. van Wyk de Vries, J. B. Murray, and V. R. Troll (2012a), A volcanotectonic survey of Ascraeus Mons, Mars, *J. Geophys. Res.*, *117*, E01004, doi:10.1029/2011JE003825.

Byrne, P. K., T. R. Watters, S. L. Murchie, C. Klimczak, S. C. Solomon, L. M. Prockter, and A. M. Freed (2012b), A tectonic survey of the Caloris basin, Mercury, *Lunar Planet. Sci.*, *43*, abstract 1722.

Byrne, P. K., A. M. C. Şengör, C. Klimczak, S. C. Solomon, and T. R. Watters (2012c), Large-scale crustal deformation on Mercury, *Lunar Planet. Sci.*, *43*, abstract 2118.

Cintala, M. J. (1992), Impact-induced thermal effects in the lunar and Mercurian regoliths, *J. Geophys. Res.*, *97*, 947–973.

Coleman, N. M. (2003), Aqueous flows carved the outflow channels on Mars, *J. Geophys. Res.*, *108*(E5), 5039, doi:10.1029/2002JE001940.

Denevi, B. W., et al. (2009), The evolution of Mercury's crust: A global perspective from MESSENGER, *Science*, *324*, 613–618.

Dombard, A. J., S. A. Hauck II, S. C. Solomon, and R. J. Phillips (2001), Potential for long-wavelength folding on Mercury, *Lunar Planet. Sci.*, *32*, abstract 2035.

Dzurisin, D. (1978), The tectonic and volcanic history of Mercury as inferred from studies of scarps, ridges, troughs, and other lineaments, *J. Geophys. Res.*, *83*, 4883–4906.

Fassett, C. I., J. W. Head, D. T. Blewett, C. R. Chapman, J. L. Dickson, S. L. Murchie, S. C. Solomon, and T. R. Watters (2009), Caloris impact basin: Exterior geomorphology, stratigraphy, morphometry, radial sculpture, and smooth plains deposits, *Earth Planet. Sci. Lett.*, *285*, 297–308.

Fassett, C. I., B. W. Denevi, J. L. Whitten, T. A. Goudge, D. M. Baker, D. M. Hurwitz, L. R. Ostrach, Z. Xiao, P. K. Byrne, and C. Klimczak (2011), Widespread and voluminous flood volcanism in the northern lowlands of Mercury revealed by MESSENGER, *Abstracts with Programs*, *43*, paper 142-6, p. 358, Geological Society of America, Boulder, Colo.

Garry, W. B., and J. E. Bleacher (2011), Emplacement scenarios for Vallis Schröteri, Aristarchus Plateau, the Moon, in *Recent Advances and Current Research Issues in Lunar Stratigraphy*, *Geol. Soc. Am. Spec. Pap*., vol. *477*, edited by W. A. Ambrose and D. A. Williams, pp. 77–93, doi:10.1130/2011.2477(03).

Ghiorso, M. S., and R. O. Sack (1995), Chemical mass transfer in magmatic processes. IV: A revised and internally consistent thermodynamic model for the interpolation and extrapolation of liquid-solid equilibria in magmatic systems at elevated temperatures and pressures, *Contrib. Mineral. Petrol.*, *119*, 197–212.

Gillis-Davis, J. J., D. T. Blewett, R. W. Gaskell, B. W. Denevi, M. S. Robinson, R. G. Strom, S. C. Solomon, and A. L. Sprague (2009), Pit-floor craters on Mercury: Evidence of near-surface igneous activity, *Earth. Planet. Sci. Lett.*, *285*, 243–250.

Glaze, L. S., S. M. Baloga, W. B. Garry, S. A. Fagents, and C. Parcheta (2009), A hybrid model for leveed lava flows: Implications for eruption styles on Mars, *J. Geophys. Res.*, *114*, E07001, doi:10.1029/2008JE003278.

Greeley, R. (1971), Lunar Hadley rille: Considerations of its origin, *Science*, *172*, 722–725.

Greeley, R., and P. D. Spudis (1981), Volcanism on Mars, *Rev. Geophys. Space Phys.*, *19*, 13–41.

Griffiths, R. W. (2000), The dynamics of lava flows, *Annu. Rev. Fluid Mech.*, *32*, 477–518.

Hauck, S. A., II, A. J. Dombard, R. J. Phillips, and S. C. Solomon (2004), Internal and tectonic evolution of Mercury, *Earth Planet. Sci. Lett.*, *222*, 713–728.

Hawkins, S. E., III, et al. (2007), The Mercury Dual Imaging System on the MESSENGER spacecraft, *Space Sci. Rev.*, *131*, 247–338.

Head, J. W., D. B. Campbell, C. Elachi, J. E. Guest, D. P. McKenzie, R. S. Saunders, G. G. Schaber, and G. Schubert (1991), Venus volcanism: Initial analysis from Magellan data, *Science*, *252*, 276–288.

Head, J. W., L. S. Crumpler, J. C. Aubele, J. E. Guest, and R. S. Saunders (1992), Venus volcanism: Classification of volcanic features and structures, associations, and global distribution from Magellan data, *J. Geophys. Res.*, *97*, 13,153–13,197.

Head, J. W., S. L. Murchie, L. M. Prockter, M. S. Robinson, S. C. Solomon, R. G. Strom, C. R. Chapman, T. R. Watters, W. E. McClintock, D. T. Blewett, and J. J. Gillis-Davis (2008), Volcanism on Mercury: Evidence from the first MESSENGER flyby, *Science*, *321*, 69–72.

Head, J. W., et al. (2009a), Volcanism on Mercury: Evidence from the first MESSENGER flyby for extrusive and explosive activity and the volcanic origin of plains, *Earth Planet. Sci. Lett.*, *285*, 227–242.

Head, J. W., et al. (2009b), Evidence for intrusive activity on Mercury from the first MESSENGER flyby, *Earth Planet. Sci. Lett.*, *285*, 251–262.

Head, J. W., et al. (2011), Flood volcanism in the northern high latitudes of Mercury revealed by MESSENGER, *Science*, *333*, 1853–1856.

Head, J. W., et al. (2012), Effusive volcanism on Mercury from MESSENGER mission data: Nature and significance for lithospheric stress state and mantle convection, *Lunar Planet. Sci.*, *43*, abstract 1451.

Hiesinger, H., J. W. Head, U. Wolf, R. Jaumann, and G. Neukum (2002), Lunar mare basalt flow units: Thicknesses determined from crater size-frequency distributions, *Geophys. Res. Lett.*, *29*, 1248, doi:10.1029/2002GL014847.

Holman, J. P. (1990), *Heat Transfer*, 7th ed., 752 pp., McGraw-Hill, New York.

Hon, K., J. Kauahikaua, R. Denlinger, and K. Mackay (1994), Emplacement and inflation of pahoehoe sheet flows: Observations and measurements of active lava flows on Kilauea volcano, Hawaii, *Geol. Soc. Am. Bull.*, *106*, 351–370.

Hulme, G. (1973), Turbulent lava flow and the formation of lunar sinuous rilles, *Mod. Geol.*, *4*, 107–117.

Hurwitz, D. M., C. I. Fassett, J. W. Head, and L. Wilson (2010), Formation of an eroded lava channel within an Elysium Planitia impact crater: Distinguishing between a mechanical and thermal origin, *Icarus*, *210*, 626–634.

Hurwitz, D. M., J. W. Head, L. Wilson, and H. Hiesinger (2012), Origin of lunar sinuous rilles: Modeling effects of gravity, surface slope, and lava composition on erosion rates during the formation of Rima Prinz, *J. Geophys. Res.*, *117*, E00H14, 619 doi:10.1029/2011JE004000.

Hurwitz, D. M., J. W. Head, P. K. Byrne, Z. Xiao, S. C. Solomon, M. T. Zuber D. E. Smith, and G. A. Neumann (2013), Investigating the origin of candidate lava channels on Mercury with MESSENGER data: Theory and observations, *J. Geophys. Res. Planets*, *118*, 471–486, doi:10.1029/2012JE004103.

Jaeger, W. L., et al. (2010), Emplacement of the youngest flood lava on Mars: A short, turbulent story, *Icarus*, *205*, 230–243.

Jarvis, R. A. (1995), On the cross-sectional geometry of thermal erosion channels formed by turbulent lava flows, *J. Geophys. Res.*, *100*, 10,127–10,140.

Kakaç, S., R. K. Shah, and W. Aung (1987), *Handbook of Single-Phase Convective Heat Transfer*, 1238 pp., John Wiley-Interscience, New York.

Kerber, L., J. W. Head, S. C. Solomon, S. L. Murchie, D. T. Blewett, and L. Wilson (2009), Explosive volcanic eruptions on Mercury: Eruption conditions, magma volatile content, and implications for interior volatile abundances, *Earth Planet. Sci. Lett.*, *285*, 263–271.

Kerber, L., J. W. Head, D. T. Blewett, S. C. Solomon, L. Wilson, S. L. Murchie, M. S. Robinson, B. W. Denevi, and D. L. Domingue (2011), The global distribution of pyroclastic deposits on Mercury: The view from MESSENGER flybys 1–3, *Planet. Space Sci.*, *59*, 1895–1909.

Kiefer, W. S., and B. C. Murray (1987), The formation of Mercury's smooth plains, *Icarus*, *72*, 477–491.

King, S. D. (2008), Pattern of lobate scarps on Mercury's surface reproduced by a model of mantle convection, *Nature Geosci.*, *1*, 229–232.

Klimczak, C., R. A. Schultz, and A. L. Nahm (2010), Evaluation of the origin hypotheses of Pantheon Fossae, central Caloris basin, Mercury, *Icarus*, *209*, 262–270.

Klimczak, C., T. R. Watters, C. M. Ernst, A. M. Freed, P. K. Byrne, S. C. Solomon, D. M. Blair, and J. W. Head (2012), Deformation associated with ghost craters and basins in volcanic smooth plains on Mercury: Strain analysis and implications for plains evolution, *J. Geophys. Res.*, *117*, E00L03, doi:10.1029/2012JE004L03.

Komatsu, G., J. S. Kargel, and V. R. Baker (1992), Canali-type channels on Venus: Some genetic constraints, *Geophys. Res. Lett.*, *19*, 1415–1418.

Komatsu, G., V. R. Baker, and V. C. Gulick (1993), Venusian channels and valleys: Distribution and volcanological implications, *Icarus*, *102*, 1–25.

Leverington, D. W. (2004), Volcanic rilles, streamlined islands, and the origin of outflow channels on Mars, *J. Geophys. Res.*, *109*, E10011, doi:10.1029/2004JE002311.

Leverington, D. W. (2007), Was the Mangala Valles system incised by volcanic flows?, *J. Geophys. Res.*, *112*, E11005, doi:10.1029/2007JE002896.

Leverington, D. W. (2009), Reconciling channel formation processes with the nature of elevated outflow systems at Ophir and Aurorae Plana, Mars, *J. Geophys. Res.*, *114*, E10005, doi:10.1029/2009JE003398.

Lipman, P. W., and N. G. Banks (1987), Aa flow dynamics, Mauna Loa 1984, *U.S. Geol. Surv. Prof. Pap.*, *1350*, 1527–1567.

Manga, M. (2004), Martian floods at Cerberus Fossae can be produced by groundwater discharge, *Geophys. Res. Lett.*, *31*, L02702, doi:10.1029/2003GL018958.

Masursky, H. (1973), An overview of geological results from Mariner 9, *J. Geophys. Res.*, *78*, 4009–4030.

Masursky, H., J. M. Boyce, A. L. Dial, G. G. Schaber, and M. E. Strobell (1977), Classification and time of formation of Martian channels based on Viking data, *J. Geophys. Res.*, *82*, 4016–4038.

McCauley, J. F., J. E. Guest, G. G. Schaber, N. J. Trask, and R. Greeley (1981), Stratigraphy of the Caloris basin, Mercury, *Icarus*, *47*, 184–202.

Melosh, H. J. (2011), *Planetary Surface Process*, 520 pp., Cambridge University Press, Cambridge, U.K.

Mouginis-Mark, P. J., L. Wilson, J. W. Head, S. R. Brown, J. L. Hall, and K. D. Sullivan (1984), Elysium Planitia, Mars: Regional geology, volcanology, and evidence for volcano-ground ice interactions, *Earth Moon Planets*, *30*, 149–173, doi:10.1007/BF00114309.

Murchie, S. L., et al. (2008), Geology of the Caloris basin, Mercury: A view from MESSENGER, *Science*, *321*, 73–76.

Murray, B. C., R. G. Strom, N. J. Trask, and D. E. Gault (1975), Surface history of Mercury: Implications for terrestrial planets, *J. Geophys. Res.*, *80*, 2508–2514.

Murray, J. B., B. van Wyk de Vries, A. Marquez, D. A. Williams, P. K. Byrne, J.-P. Muller, and J.-R. Kim (2010), Late-stage water eruptions from Ascraeus Mons volcano, Mars: Implications for its structure and history, *Earth Planet. Sci. Lett.*, *294*, 479–491, doi:10.1016/j.epsl.2009.06.020.

Nittler, L. R., et al. (2011), The major-element composition of Mercury's surface from MESSENGER X-ray spectrometry, *Science*, *333*, 1847–1850.

Oberbeck, V. R., W. L. Quaide, R. E. Arvidson, and H. R. Aggarwal (1977), Comparative studies of lunar, Martian, and Mercurian craters and plains, *J. Geophys. Res.*, *82*, 1681–1698.

Oberst, J., F. Preusker, R. J. Phillips, T. R. Watters, J. W. Head, M. T. Zuber, and S. C. Solomon (2010), The morphology of Mercury's Caloris basin as seen in MESSENGER stereo topographic models, *Icarus*, *209*, 230–238.

Pike, R. J. (1988), Geomorphology of impact craters on Mercury, in *Mercury*, edited by F. Vilas, C. R. Chapman, and M. S. Matthews, pp. 165–273, University of Arizona Press, Tucson, Ariz.

Preusker, F., J. Oberst, J. W. Head, T. R. Watters, M. S. Robinson, M. T. Zuber, and S. C. Solomon (2011), Stereo topographic models of Mercury after three MESSENGER flybys, *Planet. Space Sci.*, *59*, 1910–1917.

Prockter, L. M., et al. (2010), Evidence for young volcanism on Mercury from the third MESSENGER flyby, *Science*, *329*, 668–671.

Reidel, S. P., and Fecht, K. R. (1987), The Huntzinger flow: Evidence of surface mixing of the Columbia River basalt and its petrogenetic implications, *Geol. Soc. Am. Bull.*, *98*, 664–677.

Robinson, M. S., and K. L. Tanaka (1990), Magnitude of a catastrophic flood event at Kasei Valles, Mars, *Geology*, *18*, 902–905.

Robinson, M. S., and P. G. Lucey (1997), Recalibrated Mariner 10 color mosaics: Implications for mercurian volcanism, *Science*, *275*, 197–200.

Schenk, P. M., and D. A. Williams (2004), A potential thermal erosion lava channel on Io, *Geophys. Res. Lett.*, *31*, L23702, doi:10.1029/2004GL021378.

Schenk, P. M., R. R. Wilson, and A. G. Davies (2004), Shield volcano topography and the rheology of lava flows on Io, *Icarus*, *169*, 98–110.

Schon, S. C., J. W. Head, D. M. Baker, C. M. Ernst, L. M. Prockter, S. L. Murchie, and S. C. Solomon (2011), Eminescu impact structure: Insight into the transition from complex crater to peak-ring basin on Mercury, *Planet. Space Sci.*, *59*, 1949–1959.

Schumm, S. A. (1985), Patterns of alluvial rivers, *Annu. Rev. Earth Planet. Sci.*, *13*, 5–27.

Self, S., L. Keszthelyi, and T. Thordarson (1998), The importance of pahoehoe, *Annu. Rev. Earth Planet. Sci.*, *26*, 81–110.

Solomon, S. C., R. L. McNutt Jr., and L. M. Prockter (2011), Mercury after the MESSENGER flybys: An introduction to the special issue of *Planetary and Space Science*, *Planet. Space Sci.*, *59*, 1827–1828.

Solomon, S. C., et al. (2012), Long-wavelength topographic change on Mercury: Evidence and mechanisms, *Lunar Planet. Sci.*, *43*, abstract 1578.

Stockstill-Cahill, K. R., T. J. McCoy, L. R. Nittler, S. Z. Weider, and S. A. Hauck II (2012), Magnesium-rich crustal compositions on Mercury: Implications for magmatism from petrologic modeling, *J. Geophys. Res.*, *117*, E00L15, doi:10.1029/2012JE004140.

Strom, R. G., N. J. Trask, and J. E. Guest (1975), Tectonism and volcanism on Mercury, *J. Geophys. Res.*, *80*, 2478–2507.

Trask, N. J., and J. E. Guest (1975), Preliminary geologic terrain map of Mercury, *J. Geophys. Res.*, *80*, 2461–2477.

Walker, G. P. L. (1991), Structure, and origin by injection of lava under surface crust, of tumuli, "lava rises", "lava-rise pits", and "lava-inflation clefts" in Hawaii, *Bull. Volcanol.*, *53*, 546–558.

Watters, T. R. (1988), Wrinkle ridge assemblages on the terrestrial planets, *J. Geophys. Res.*, *93*, 10,236–10,254.

Watters, T. R., S. C. Solomon, C. Klimczak, A. M. Freed, J. W. Head, C. M. Ernst, D. M. Blair, T. A. Goudge, and P. K. Byrne (2012), Extension and contraction within volcanically buried impact craters and basins on Mercury, *Geology*, *40*, 1123–1126.

Weider, S. Z., L. R. Nittler, R. D. Starr, T. J. McCoy, K. R. Stockstill-Cahill, P. K. Byrne, B. W. Denevi, J. W. Head, and S. C. Solomon (2012), Compositional heterogeneity on Mercury's surface revealed by the MESSENGER X-Ray Spectrometer, *J. Geophys. Res.*, *117*, E00L05, doi:10.1029/2012JE004153.

Whitford-Stark, J. L., and J. W. Head (1977), The Procellarum volcanic complexes: Contrasting styles of volcanism, *Proc. Lunar Sci. Conf.*, *8th*, 2705–2724.

Wilhelms, D. E. (1976), Mercurian volcanism questioned, *Icarus*, *28*, 551–558.

Williams, D. A. (1998), Analytical/numerical modeling of the emplacement and erosional potential of Archean and Proterozoic komatiitic lava flows, Ph.D. thesis, University of Alabama, Tuscaloosa, Ala.

Williams, D. A., S. A. Fagents, and R. Greeley (2000), A reassessment of the emplacement and erosional potential of turbulent, low-viscosity lavas on the Moon, *J. Geophys. Res.*, *105*, 20,189–20,205.

Williams, D. A., R. C. Kerr, C. M. Lesher, and S. J. Barnes (2001a), Analytical/numerical modeling of komatiite lava emplacement and thermal erosion at Perseverance, Western Australia, *J. Volcanol. Geotherm. Res.*, *110*, 27–55.

Williams, D. A., A. G. Davies, L. P. Keszthelyi, and R. Greeley (2001b), The summer 1997 eruption at Pillan Patera on Io: Implications for ultrabasic lava flow emplacement, *J. Geophys. Res.*, *106*, 33,105–33,119.

Williams, D. A., R. Greeley, E. Hauber, K. Gwinner, and G. Neukum (2005), Erosion by flowing martian lava: New insights for Hecates Tholus from Mars Express and MER data, *J. Geophys. Res.*, *110*, E05006, doi:10.1029/2004JE002377.

Williams, H., and A. R. McBirney (1979), *Volcanology*, 397 pp., Freeman, Cooper and Co., San Francisco, Calif.

Zimbelman, J. R. (1998), Emplacement of long lava flows on planetary surfaces, *J. Geophys. Res.*, *103*, 27,503–27,516.

Zuber, M. T., et al. (2012), Topography of the northern hemisphere of Mercury from MESSENGER laser altimetry, *Science*, *336*, 217–220, doi:10.1126/science.1218805.